

Abstract

Lightning strikes produce electromagnetic waves, now referred to as sferics, in the very low frequency (VLF, 3–30 kHz) and the extremely low frequency (ELF, 3–3k Hz) bands. Within these frequency bands, the Earth and ionosphere form a waveguide in which sferics propagate long distances with low attenuation. The structure of the received sferic waveform is mainly a function of propagation distance and the waveguide's parameters. This suggests that each observed sferic waveform contains information about the distance that this sferic has propagated which can be used to geolocate lightning. There are various approaches for analyzing received sferics, which mostly rely on measurements from multiple stations. However, in these methods, each station imposes an additional cost for building, maintenance, and synchronization. Here we present a novel method to estimate both the emission time and location of lightning, which works by measuring sferics recorded at a single station. We first process the sferic waveforms to obtain the arrival times of the VLF and ELF radiation components which propagate with different speeds. Once these two separate arrival times are determined, we use them to approximate the distance the sferic propagated in the Earth-ionosphere waveguide. We have used this novel method in combination with a method to find sferic direction to geolocate a significant number of lightning strikes for July 4, 2013. Using this proposed method, the distance of propagation estimates are accurate to within 6.7% of the NLDN determined propagation distance and the direction of propagation estimates are accurate to within $\sim 1.3\%$ of the NLDN determined direction.

1 Introduction

Electromagnetic waves originating from lightning are called radio atmospheric, or sferics. The VLF and ELF components of the sferics propagate global distances through the Earth-ionosphere waveguide. A number of studies have used these components individually or together to geolocate lightning from recorded sferic data (Said, R. *et al.*, 2010; Price, C. *et al.*, 2002). Figure 1 shows the VLF and ELF components of a typical sferic waveform. The VLF component, highlighted in pink on the left, is the initial burst, which is followed by the ELF component, highlighted on the right. In Figure 1, the magnitudes of both components are normalized (the plotted magnitude is $\frac{M - \text{mean}(M)}{\text{max}(M)}$, where M is the measured time-domain signal amplitude). The VLF and ELF components of different sferics vary in time duration, but in general the VLF component is considerably shorter than

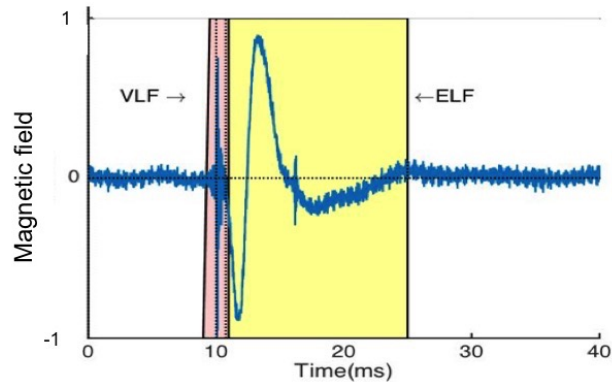


Figure 1. An example of a spheric waveform and the two associated VLF and ELF components (recorded at Arrival Height on June 6, 2013 at 06:30 A.M.)

the ELF component. The data set used in this paper were recorded at two stations, one located at Arrival Height, Antarctica (78°S , 167°E), and the other at Sondrestrom, Greenland (66.99°N , 50.95°W), on June 6th and July 4th, 2013, respectively. In each of the stations, sferics were measured by two orthogonal magnetic loop antennas in North-South (NS) and East-West (EW) geomagnetic directions. The data are recorded with a sampling frequency of 100 kHz, and antennas are capable of measuring horizontal magnetic field in frequencies ranging from 300 Hz to 40 kHz.

Using the above data and our proposed method, we first estimated the distances of the lightning strikes and then compared the accuracy of our estimations with the locations estimated by the National Lightning Detection Network's (NLDN) multi-station method.

2 Current Lightning Location Methods

Several prior studies have attempted to utilize observed sferics at multiple ground stations to locate lightning. Some of them are based on multi station detections and use a central processor to employ Time of Arrival (TOA) and Magnetic direction finding (MDF) techniques (Nag *et al.*, 2015, Said, R., 2017). NLDN and the Global Lightning Detection Network (GLD360) are examples of multi-station networks used to locate lightning. NLDN, operated by Vaisala, Inc., employs a network of low Frequency (LF) and VLF sensors to provide lightning location within the continental United States. Using NLDN, the arrival time and azimuth are measured with accuracies of $1.5 \mu\text{s}$ and 1° , respectively (Cummins & Murphy, 2009). The detection efficiency is estimated to be $\sim 60\text{--}76\%$ for

65 cloud to ground strokes . The median location error, as an important evaluation metric
66 (*Murphy, M*, 2018), was reported around 308 m (*Nag et al.*, 2011). In GLD360, each sta-
67 tion correlates observed sferic data with a waveform-bank. Multiple stations then send
68 their results to a central processor to approximate the lightning's time and locations. This
69 method achieves 57 % flash detection efficiency and ~2–5 km accuracy (*Said,R et al.*;
70 2010; *Said,R et al.*, 2013).

71 Alternative methods exist to locate lightning using mostly VLF measurements from
72 a single station. For example in (*Byerley, III et al.*, 1991) the ratio between radiation field
73 component (E_r) and an electrostatic field component (E_s) is used for close-range lightning
74 detection. The ratio of electric and magnetic fields or wave impedance also have been
75 used to estimate propagation distance using a single station (*Burke et al.*, 1995). However,
76 these methods require the availability of both electric and magnetic field antennas, intro-
77 ducing additional cost and complexity in each station, which also is a concern in multi-
78 station locating methods. *Ramachandran, V, et al.* ,2007 described another method which
79 works based on lightning-generated VLF sferics received in a single station. The reports
80 8.8% average distance estimation error, but it doesn't benefit from using ELF components
81 of the sferic to improve distance estimations.

82 On the other hand, Wait developed a theory proposing that lightning can be located
83 by examining the structure of recorded sferic data from a single location. *Wait, J. R.*,
84 1960 also proposed a theory to estimate propagation distance by modeling the ELF com-
85 ponent of the sferics.

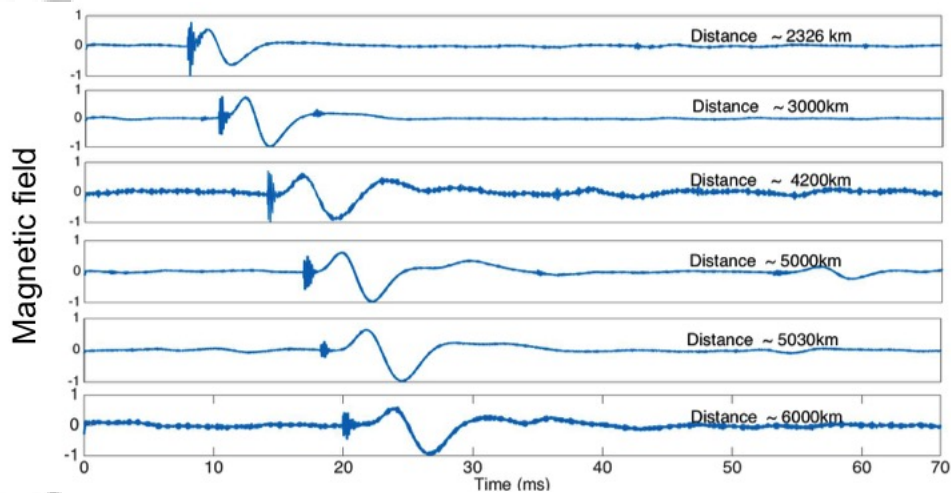
86 However, Wait's method suffers from limited accuracy. An average error of 45.1%
87 for daytime conditions with a standard deviation of 13.8% is reported for his method
88 (*Mackay, C.E.J et al.*, 2010). Wait assumed a certain analytical form for the lightning cur-
89 rent moment, which non-ideally can be used to model the ELF component of the sferic.
90 Later more accurate approximation for source current moment was introduced by *Cummer*
91 *and Inan, 2000* and used by *Mackay, C.E.J et al.*, 2010 which shows an improvement in
92 lightning distance estimation. However this improvement is also limited by assumptions
93 made regarding the source and current of the lightning discharge.

94 On the other note, Ogawa has found that by examining the background noise in 1
95 Hz to 11 kHz, it is possible to observe a secondary waveform caused by the same light-
96 ning strikes. The secondary (antipodal) waveform results from the sferic propagating along

97 the opposite direction around the world. With data from the direct and secondary wave-
 98 forms, lightning location can be estimated (*Ogawa et al.*, 2007), though in many cases it
 99 is hard identify the secondary waveforms . To overcome these problems, we introduce a
 100 lightning detection method based on observations from a single station that do not suffer
 101 from these limitations.

102 3 Evolution of sferics time domain structure with distance

105 Before introducing our method, we begin by inspecting some recorded sferics shown
 in Figure 2. By evaluating the data in this figure, we can make several key observations



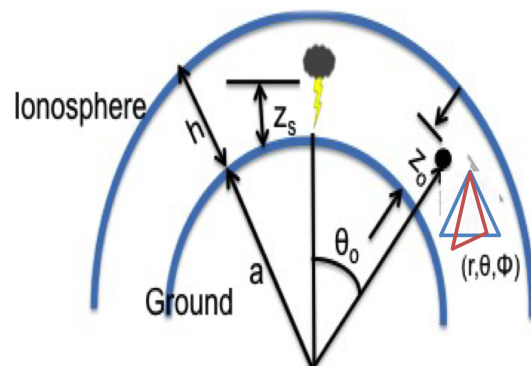
103 **Figure 2.** Example of sferics over different distances recorded during the night. Data recorded at Sondre-
 104 strom station.

106 that will form the basis of our proposed algorithm. Each row in the figure corresponds to
 107 a lightning discharge reported by the NLDN dataset. We also used this dataset to calcu-
 108 late the propagation distance and to determine whether the sferic propagated during the
 109 daytime or nighttime. All of the sferics shown in Figure 2 propagated during the night.
 110 The zero point for each row is an NLDN time estimate for a lightning strike. Although
 111 the sferic magnitude is generally attenuated over propagation distance, here the magni-
 112 tudes have been normalized. Therefore, the magnitude attenuation is not shown in Fig-
 113 ure 2. This normalization will help us to see the patterns and variations in the waveform
 114 structure for different propagation distances, which is a key for our method. There are two
 115 key observations to make: as the propagation distances increase, 1) the time interval be-
 116

117 between the zero time and the spheric start point increases, and 2) the separation time between
 118 the VLF component (initial burst) and the ELF component (subsequent component) also
 119 increases. In the following sections, we will show that these two time values are both pro-
 120 portional to propagation distance. This, along with phase velocity derivations described in
 121 section 4 and 5, will be the basis of our method to estimate the propagation distances.

122 **4 Galejs's model for the Earth-ionosphere wave guide**

124 In this work we use phase velocities derived from the Earth-ionosphere model de-
 125 veloped by Galejs. Galejs formulated a model to study wave propagation in the spheri-
 126 cal shell between the Earth and ionosphere (*Galejs, J., 1972*). The model makes a number
 127 of simplifying assumptions. It assumes the Earth and ionosphere boundaries are concen-
 128 tric spheres forming a spherical waveguide. The ionosphere is assumed to be a sharply
 129 bounded and homogeneous ionized medium. Galejs further assumes the height and con-
 130 ductivity of the ionosphere remain constant through the propagation path. Figure 3 illus-
 131 trates this model with two boundaries located at $r = a$ and $r = a + h$, where a is Earth's
 132 radius and h is the ionosphere height. The source as a vertical dipole is located on the
 133 ground at $\theta = 0$, $r = a + Z_s$, and the receiving antenna (shown as orthogonal loops) is
 located on the ground at $\theta = \theta_0$, $r = a + Z_o$. Since the ionization level of the ionosphere



123 **Figure 3.** Geometry of the Earth-ionosphere spherical shell

134 is different in day and night, the height and conductivity of the ionosphere vary in daytime
 135 and nighttime (*Wait, J. R., 1960*). Considering this fact, in this paper and in the Galejs
 136 model, different values are assumed for the height and conductivity of the ionosphere de-
 137 pending on whether sferics propagate during day or night. During the day h is set to 70
 138

139 km and the conductivity of the ionosphere is assumed to be 10^{-6} S/m. At night h is set
 140 to 85 km and the conductivity of the ionosphere is assumed to be 10^{-5} S/m. The ground's
 141 conductivity is assumed 10^{-3} S/m for day and night. The solution of radial fields observed
 142 at $r = a + Z_o$ is expressed in terms of spherical Bessel functions as :

$$143 \quad R(r) = r[Ah_\nu^{(1)}(u) + Bh_\nu^{(2)}(u)] \quad (1)$$

144 where:

$$145 \quad h_\nu^m(u) = \left(\frac{\pi}{2u}\right)^{0.5} H_{\nu+0.5}^m(u) \quad (2)$$

146 and $H_{(\nu+0.5)}^m(u)$ is the Hankel function of kind m and order $\nu + 0.5$, $u = k_0 r$ and k_0 is the
 147 wave number and is equal to

$$148 \quad k_0 = \omega\sqrt{\mu_0\epsilon_0} \quad (3)$$

149 μ_0 and ϵ_0 are the permeability and permittivity of free space, respectively. Due to lack of
 150 simple representations for the spherical Bessel functions of large order ν and u , a solu-
 151 tion for approximation for thin shell was developed , where $\frac{h}{r} \rightarrow 0$. The factor r is also
 152 approximated by the average value in the shell ($r_m = a + 0.5h$). With this assumption,
 153 equation (1) reduces to equation (4) as below:

$$154 \quad R = Aexp(iKr) + Bexp(-iKr) \quad (4)$$

155 where

$$156 \quad K^2 = k_0^2[1 - (aS/r_m^2)] \quad (5)$$

157 and S is the propagation parameter, which can be interpreted as the ratio between the
 158 wave number along the surface of the earth k_θ and the wave number of the free space k_0 .

159 In this paper, S is used to find the velocity of both the VLF and ELF components of sfer-
 160 ics. Galejs defined S using modal equation of T.M. modes for the VLF range in equation

161 (6):

$$162 \quad S = \frac{r_m}{a} \sqrt{1 - \left[\frac{(n-0.5)\pi}{k_0 h}\right]^2} \quad (6)$$

163 where n is T.M. mode number and can be one or an arbitrary integer. Galejs shows equa-
 164 tion (6) is strictly valid for a conducting ground surface and a perfectly reflective iono-
 165 sphere. However, these assumptions may idealize the boundaries in the VLF range and the
 166 results may slightly diverge from observations. In the ELF range, where only the TEM
 167 mode propagates, the waveguide boundaries appear as nearly perfect conductors and equa-
 168 tion (6) can be reduced to equation (7):

$$169 \quad S = \frac{r_m}{a} \sqrt{1 + \frac{i(\Delta_e + \Delta_g)}{k_0 h}} \quad (7)$$

170 where

$$171 \Delta_e = \sqrt{\frac{\omega \epsilon_0}{\omega \epsilon_0 \epsilon_i + i \sigma_i}} \quad (8)$$

172 and

$$173 \Delta_g = \sqrt{\frac{\omega \epsilon_0}{\omega \epsilon_0 \epsilon_g + i \sigma_g}} \quad (9)$$

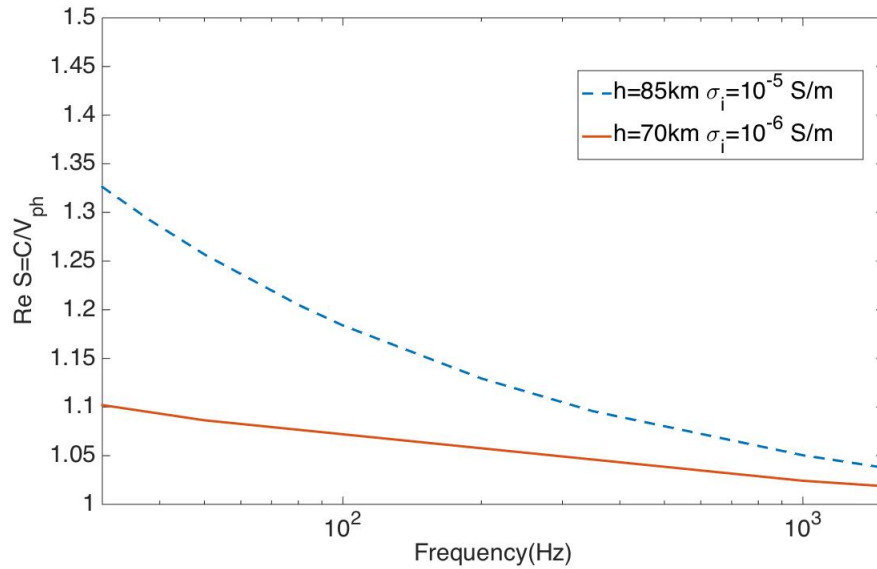
174 Δ_e and Δ_g represent the normalized impedances for the ionosphere and ground, respec-
 175 tively. ϵ_i , ϵ_g and ϵ_0 are the permittivity of the ionosphere, ground, and free space, respec-
 176 tively. σ_i and σ_g are the electrical conductivity of the ionosphere and ground, respec-
 177 tively. Having defined S , Galejs went on to derive the phase velocities. In our method,
 178 the phase velocities are essential parameters for estimating lightning distances. In the next
 179 section we present the phase velocities for the VLF and ELF components of sferics using
 180 Galejs's model.

181 5 Modeling waves 's phase velocities

182 The phase velocity is inversely related to the real part of the propagation parameter
 183 as follows:

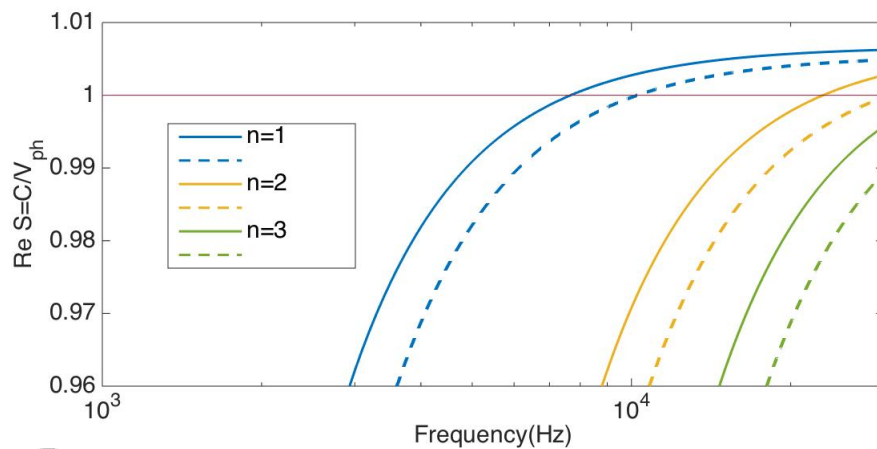
$$184 V_{ph} = \frac{c}{\text{Real}(s)} \quad (10)$$

186 where $C = \frac{1}{\sqrt{\mu_0 \epsilon_0}}$ is the free-space velocity of electromagnetic waves. Since the Galejs
 187 model is most accurate at lower frequencies, where the height of the waveguide is smaller
 188 than the wavelength (*Galejs, J. et al., 1972*), we can confidently apply this model to obtain
 189 the propagation parameter for low frequency bands. Figures 4 and 5 show S in ELF and
 190 VLF frequencies, respectively. Later we use these graphs along with equation (10) to find
 191 the phase velocity for these components of the sferic. Using equation (7) we calculated
 192 the real part of propagation parameter in the ELF frequency band for both daytime and
 193 nighttime, which are shown in Figure 4. It follows from equation (7) and equation (3) that
 194 for an increase in frequency, S will decrease. Figure 4 shows this as a downward trend in
 195 S over frequency. The first cut off frequency for the Earth-ionosphere waveguide is 1580
 196 Hz (*Inan, et al., 2000*). As shown in Figure 4, at frequencies less 1580 Hz, S is greater
 197 than one. Since S is greater than one, according to Equation (10), the phase velocity in
 198 the ELF range is less than c . However, as the waveguide boundaries become perfect con-
 199 ductors the phase velocity of the ELF waves becomes nearly equal to c . This is because,
 200 in perfect conductors, normalized impedances (Δ_e and Δ_g) approach zero, causing S to
 201 approach one. Figure 5 shows the propagation parameter of the VLF waves, calculated
 202 using Equation (6), with different values for daytime and nighttime. The value reported in



185 **Figure 4.** Propagation parameter of the ELF waves, red for day and blue for night

203 this graph is consistent with phase values reported by *Wait, J. R., 1970*. In contrast with
 204 the ELF range, the propagation parameter in the VLF range shows different behavior. As
 205 shown in Equation (6), an increase in frequency will result in an increase in S . This ac-
 206 counts for the upward trend observed in Figure 5.



207 **Figure 5.** Propagation parameter of the VLF waves in the first three modes, dashed line for day and
 208 line for night

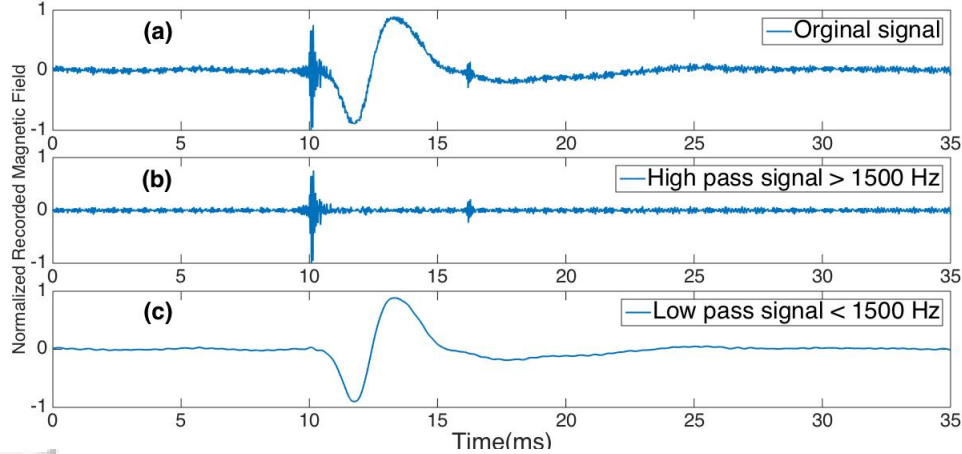
209 One interesting observation from Equation (6): S is imaginary for lower frequencies
210 and, as a result, the waves in that frequency range are severely attenuated. But as the fre-
211 quency approaches the cutoff frequencies, $k_0 = k_c = \frac{(n-0.5)\pi}{h}$ and S approaches zero. Thus,
212 according to Equation (10), the phase velocity will be infinite at the cutoff frequencies. In
213 the frequencies higher than the cutoff frequencies, S will gradually becomes greater than
214 one, and when that occurs, the phase velocity becomes less than c .

215 **6 Methodology**

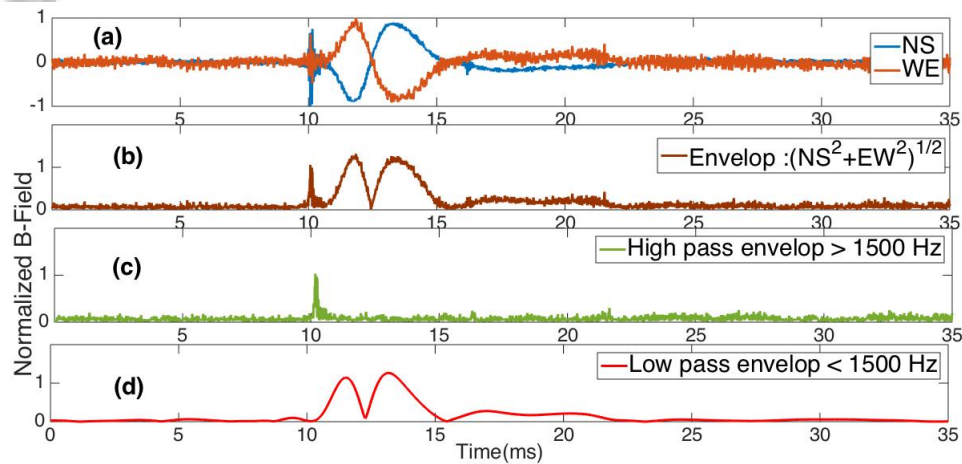
216 Section 5 described a model how to obtain the phase velocities for the VLF and
217 ELF components of the sferic. These values will be used as inputs in our method to esti-
218 mate lightning distance. Our methodology can be divided into three main steps: 1) Sferic
219 identifications in the recorded data 2) Distance and time estimation of lightning using ELF
220 and VLF components of the identified sferic 3) Direction estimation. Finally, we employ
221 all three of these steps to geolocate the lightning. Each of these steps are described in the
222 following sections.

223 **6.1 Sferic identification in recorded data**

229 As mentioned before, the method presented here to find the lightning emission time
230 and location is based on characteristics of the associated ELF and VLF components of
231 sferics. Prior to using sferics, the ELF and VLF components must first be identified and
232 isolated in the recorded data. An example of this isolation process is shown in Figure 6.
233 Figure (6a) illustrates a typical sferic waveform generated by lightning in approximately
234 300Hz-40 kHz frequency range. Figures (6b) and (6c) show the isolated VLF and ELF
235 components of the same sferic, after passing it through high- and low-pass filters, respec-
236 tively. We also eliminated the phase shifts introduced by filters by compensating the group
237 delays. The waveform shown above was received by a NS directed antenna . However,
238 the closer the sferic 's arrival direction is to the EW direction, the less the NS antenna
239 will be able to capture the signal. As a result, to capture a sferic coming from any pos-
240 sible direction, we need to consider recorded data from the antenna directed in EW, the
241 orthogonal direction, as well. Figure (7a) shows the sferic displayed in Figure (6) but
242 now includes both NS and EW directions, shown in red and blue, respectively. To iden-
243 tify a sferic's waveform coming from any direction, we calculate the envelope of the signal
244 $(NS^2 + EW^2)^{0.5}$ from the recorded data, shown in Figure (7b). To determine the arrival



224 **Figure 6.** A typical sferic waveform recorded in the Arrival Height station (a), the high-pass waveform
 225 (>1500 Hz; VLF component) (b), and the low-pass waveform (<1500 Hz; ELF component) (c).



226 **Figure 7.** The same recorded sferic as in Figure 6 now including NS and EW directions (a), envelope in
 227 300 Hz– 40 kHz band (b), high-pass envelope (>1500 Hz; VLF component) (c), and the low –pass envelope
 228 (<1500 Hz; ELF component) (d).

245 time of the VLF component (t_{VLF}), we passed the envelope signal through a high pass
 246 filter with a cutoff frequency of 1500 Hz. The high- pass envelope of the corresponding
 247 sferic is shown in Figure (7c). Using the high-pass envelope, we determine t_{VLF} to be
 248 the global maximum point in that envelope. To find the arrival time of the ELF compo-
 249 nent (t_{ELF}), we passed the envelope signal through a low pass filter using the same cut-
 250 off frequency as the VLF component. The low pass envelope of the corresponding sferic

is shown in Figure (7d). We also defined the first global peak as the arrival time of the spheric.

It should be noted that the detection efficiency of proposed distance estimation method is limited to the percentage of sferics with clear ELF components. There exists a number of factors that limits the percentage of clear sferics. One of these factors is the interference with other recorded sferics which reduces the percentage of clear and usable sferics. Mackay C.E.J, et al., 2012 shows that on average, 70 percent of the recorded sferics are interference-free. Another limiting factor is noise threshold. For a spheric to be detectable in a particular station, the spheric power must be higher than the noise level threshold in that station. It means the magnitude of peak current of the spheric should be greater than the station noise cutoff and the attenuation of propagation path.

6.2 Distance Estimation algorithm

All of the previous sections have provided us with required inputs for a novel algorithm that is described in the following sections. To start, assume that the lightning discharge happened at $t_{initial}$ at d distance from our receiver. And also assume t_{VLF} and t_{ELF} are the arrival times of the VLF and ELF components, respectively. Also assume that the waves in ELF and VLF bands propagate along the same path to reach the antennas. Given these parameters and according to the time-velocity relationship:

$$V_{VLF} = \frac{d}{t_{VLF} - t_{initial}} \quad (11)$$

$$V_{ELF} = \frac{d}{t_{ELF} - t_{initial}} \quad (12)$$

Solving Equation (11) and (12) leads to:

$$t_{initial} = \frac{t_{VLF}V_{VLF} - t_{ELF}V_{ELF}}{V_{VLF} - V_{ELF}} \quad (13)$$

$$d = a(t_{ELF} - t_{VLF}) \quad (14)$$

Where a is a constant and

$$a = \frac{V_{ELF}V_{VLF}}{V_{VLF} - V_{ELF}} \quad (15)$$

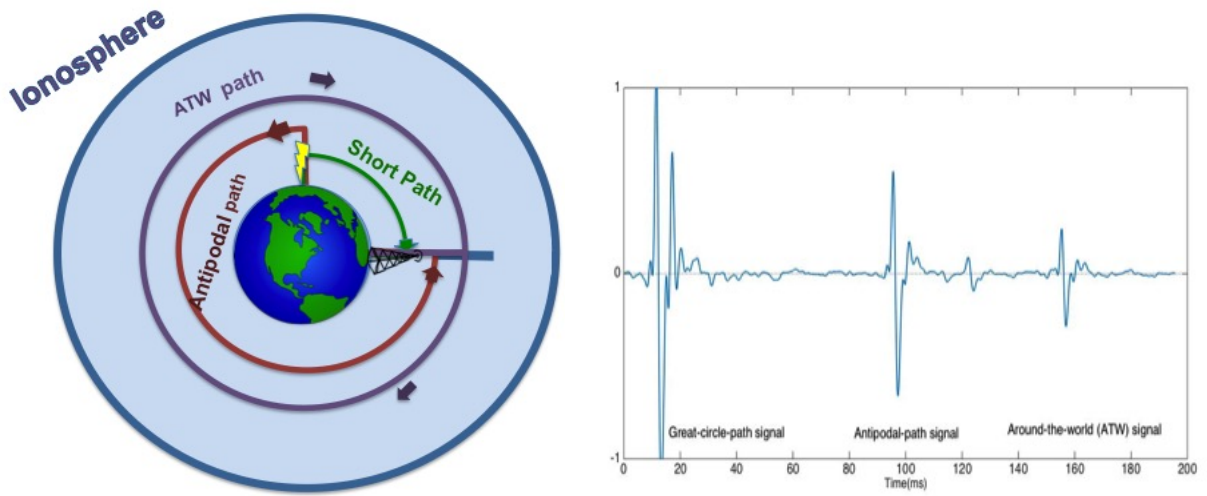
In equation (14), $t_{ELF} - t_{VLF}$ is the separation time between the arrival of waves in the ELF and the VLF bands and can be calculated from the waveform's characteristics as described in section 6-1. As deduced from equation (13) and equation (14), we can see that

281 only the velocity and arrival times for the ELF and VLF components from a single station
282 are necessary to find emission time and the propagation distance of the lightning strikes.
283 This frees us from the traditional locating methods, which required recording data from
284 multiple stations. Since the profile of the ionosphere differs during daytime and night
285 time, characteristics of a sferic also varies depending on whether it propagated during the
286 day, at night, or across the day-night terminator. The proposed distance estimation method
287 assumes the sferic propagated during the day or at night. When the sferic crosses the day-
288 night terminator, signal propagation should be modeled over nonuniform waveguide which
289 leads to a much more complex problem. As a possible solution, propagation parameters
290 can be averaged to determine attenuation rates and phase velocities of sferics crossing the
291 day-night terminator. A more complex solution involves modeling attenuation as a depen-
292 dent of propagation distance and time of day (*Mackay, C.E.J et al(2010)*).

293 **6.3 Additional Distance Estimation method**

294 In certain circumstances, there is an additional method that can be used along with
295 our method. When these two methods are used together, they yield more accurate distance
296 approximations from recorded data. Ogawa found that with a strong lightning strike it is
297 possible to observe a secondary waveform caused by the same lightning strike (*Ogawa,*
298 *et al., 2007*). These antipodal waves propagate in the opposite direction across the globe
299 (Figure 8). The difference in arrival times between the antipodal wave and direct wave
300 can also be used to estimate the distance between antennas and individual lighting occur-
301 rences.

304 Figure 8 shows an ELF sferic generated by a single lightning return stroke, which
305 has three noticeable components. The first burst is correlated to the shortest path from the
306 lightning to the receiver; antipodal path generate the second burst and the third burst is
307 the shortest path and a delay from one around-the-world (ATW) path. Since the antipodal
308 wave needs to travel at least half of Earth's circumference ($\sim 20Mm$), the VLF compo-
309 nent of the lightning will be significantly attenuated. However, the ELF component will
310 not display the same level of attenuation and, because of that it should generally be visible
311 in the spectrum data radiated by antipodal waves. Considering this fact, the time –velocity
312 relationship for the direct and antipodal waves are shown in equation (16) and (17):



302 **Figure 8.** The illustrations of Short path and antipodal path (a), a particular (ELF) spheric waveform with
 303 three noticeable bursts recorded in the Arrival Height station (b)

$$313 \quad V_{ELF} = \frac{d}{t_{Direct} - t_{initial}} \quad (16)$$

$$314 \quad V_{ELF} = \frac{40M - d}{t_{Antipodal} - t_{initial}} \quad (17)$$

316 Where V_{ELF} is the phase velocity of waves in ELF range d is the shortest distance be-
 317 tween return stroke and receiver antenna. t_{Direct} and $t_{Antipodal}$ are correlated to direct
 318 and antipodal waves respectively. Solving equations (16) and (17) for d leads to equation
 319 (18):

$$320 \quad d = 20Mm - \frac{V_{ELF}}{2} (t_{Antipodal} - t_{ELF}) \quad (18)$$

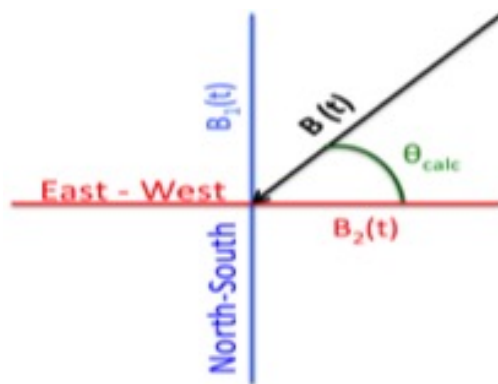
321 In conclusion, since both Equation (14) and (18) estimate propagation distance separately,
 322 using both equations and averaging their distance estimations can potentially lead to a
 323 more accurate result. While the Ogawa method is also a single station method for es-
 324 timating the propagation distances, it has some restrictions that limit its use when com-
 325 pared to our method. In particular it is limited to cases where lightning strikes are strong
 326 enough that attenuated ELF waves are still visible in the recorded data. Another limitation
 327 is that this method is restricted to cases where the lightning occurred not too close to the
 328 receiver, because in this case the antipodal wave will be highly attenuated and not visible
 329 in the received data. The other disadvantage of Ogawa method is that in his equation, the

330 velocity of the waves stays the same for the whole propagation path. However, the antipo-
 331 dal waves must cross the day-night terminator, which requires considering different wave
 332 velocities for day and night.

333 In comparison to single station method presented in Ogawa. et al (2007), the pro-
 334 posed method described in section 6.2 does not require observing antipodal peak on the
 335 spheric's structure, making it more widely applicable. Also compared to (Mackay C.E.J,
 336 et al., 2012), another single station method, this method is less resource intensive and re-
 337 quires less processing cycles and memory usage.

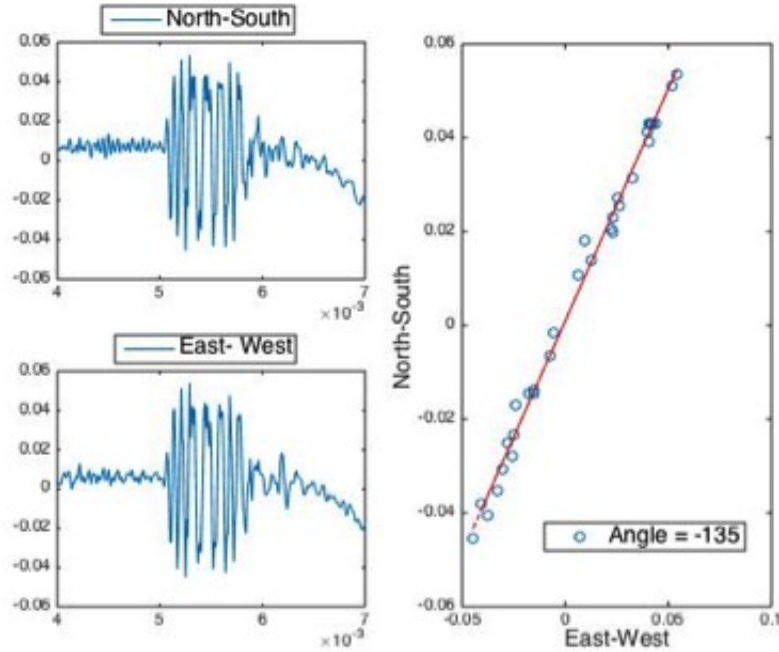
338 6.4 Direction estimation

345 Given the estimated distance between lightning strike and receiver, to obtain the lo-
 346 cation of the lightning we only need to find the spheric's incoming direction. Horizontal
 347 magnetic field measurements could be used in the magnetic direction finding(MDF) of
 348 lightning discharges (Füllekrug, M, 2017). To do this, we use MDF method for the sin-
 349 gular station which was introduced by Said, R. K. et al., 2010. This method also uses data
 350 from two orthogonal loop antennas that are positioned in NS and EW directions. The in-
 351 coming spheric excites the NS and EW antenna, and as shown in Figure 9, inducing signal
 $B_1(t)$ and $B_2(t)$ in NS and EW antennas respectively Since the ratio of $B_1(t)$ and $B_2(t)$ is



339 **Figure 9.** An illustration for finding the direction of lightning

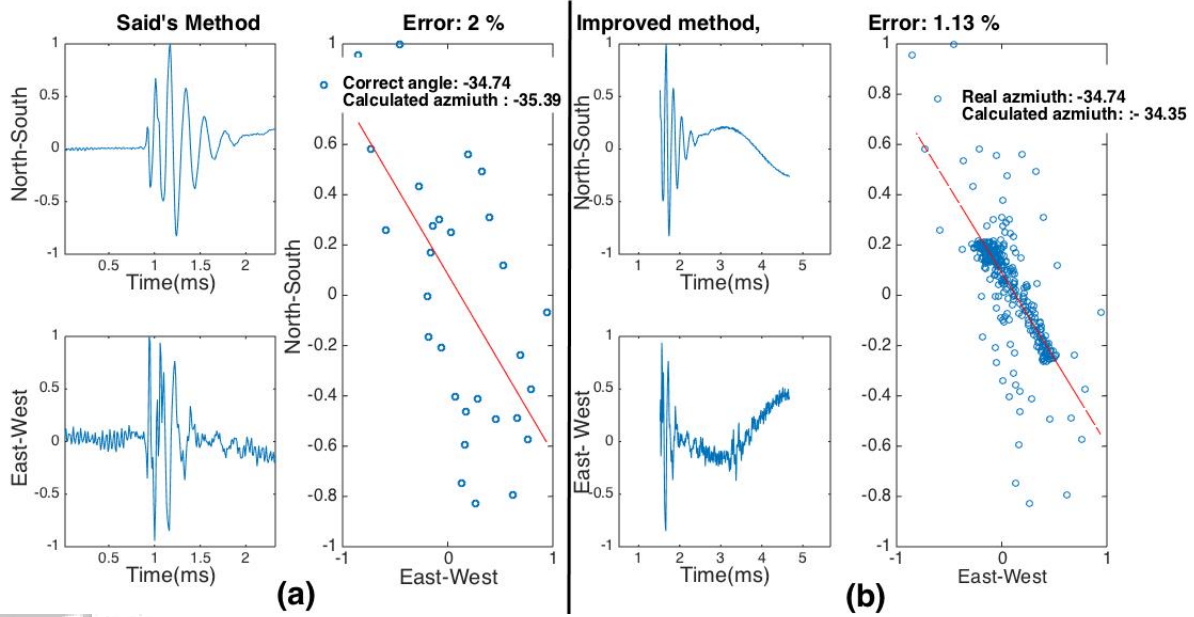
352 proportional to the tangent of the azimuth, they can be sampled and used to find the in-
 353 coming direction of the spheric. Figure 10 illustrates an implementation of Said, R. K. et
 354 al.'s, 2010 method using our data. As the method is developed for the VLF component
 355 of the spheric, we first isolated the VLF component by passing it through a high pass fil-
 356



340 **Figure 10.** An example of direction finding algorithm. North-South and East-West measurements are plotted
 341 versus time in left-hand figures. The right hand figure display North-South vs East-West recording and the
 342 best linear fitting in solid line. The azimuth of the sferics calculated as $\theta_{calc} = 45$.

357 ter (1500 Hz). After isolation, we plotted the NS recording against the EW recording for
 358 the first $500\mu s$. The tangent of the azimuth is the slope of the least-squared fitting line of
 359 the plot. However, if the data recorded from one of the antennas is noisy the accuracy of
 360 this method will dramatically drop. We found out that an improvement can be achieved
 361 in direction estimation if we instead consider sferic waveform in full bandwidth and not
 362 limit ourselves to only the VLF part of the sferics. This would add more data points to
 363 the model and potentially helps fitting a more accurate line. Figure 11 illustrates an our
 364 improvement on Said's method on a noisy recorded data. One potential limitation to this
 365 method could be the cases where the ELF component has a lower SNR than the VLF
 366 component, where considering noisy ELF data, could drop the accuracy of fitting line.
 367 Also since the crossed antennas at the site are never perfectly aligned to the geographi-
 368 cal North-South and East-West, we used equation (19) to compute a corrected arrival az-
 369 imuth, θ_{corr} , using the calculated azimuth, θ_{calc} , and the correction factors specific to the
 370 recording site.

$$371 \quad \theta_{corr} = \tan^{-1} \left[\alpha \frac{\tan(\theta_{calc})}{\cos \xi} - \tan \xi \right] + \phi \quad (19)$$



343 **Figure 11.** Direction approximation for a sample spheric recorded in Sondrestrom using Said, R. et al., 2010
 344 method (a), using proposed MDF method (b)

372 For results presented in this paper, which are recorded at Sondrestrom, correction factors
 373 are as follow: $\alpha = 1$, $\xi = 20^\circ$ and $\phi = 79^\circ$ (Mackay, C.E.J et al., 2012).

374 7 Results

375 To estimate the distance of propagation, we employed our proposed method (de-
 376 scribed by equation (14)) along with the Ogawa method (described by equation (17))
 377 when possible. By using both equations and averaging their distance estimations, we can
 378 potentially gain a more accurate result. However, the Ogawa method could only be ap-
 379 plied to a limited number of sferics where special conditions mentioned in section 6-3
 380 are satisfied. Method correctness requires that the velocity computations and arrival-time
 381 measurements be computed in the same frequency, since both are frequency-dependent. In
 382 this work, we have arbitrarily selected 500 Hz and 30kHz as operating frequencies for the
 383 ELF and VLF computations, respectively. To use our proposed method we need to find
 384 the constant a (equation (14)). This constant is a function of the ELF and VLF veloci-
 385 ties, which are themselves a function of their respective propagation parameters. For the
 386 ELF component, we applied $f=500$ Hz, $\sigma_i = 10^{-5}$ S/m, and we obtained $S = 1.05$ for

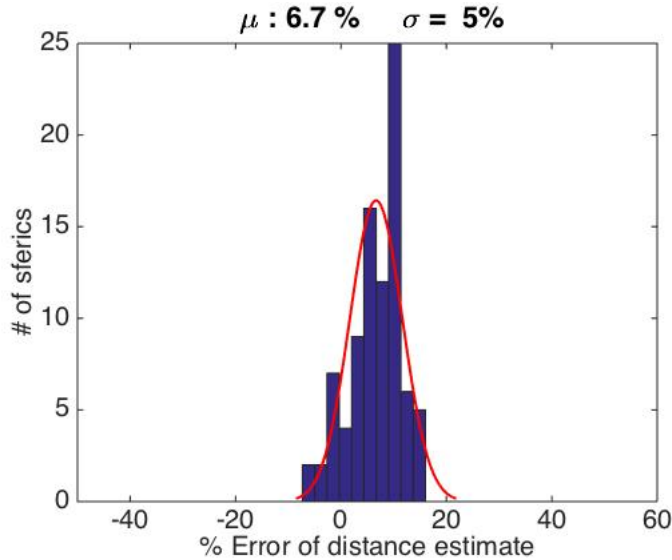
387 the nighttime profile. Substituting the S value in equation (10) gives a phase velocity of
 388 $\sim 2.85 \times 10^8$ m/s.

389 For the VLF component, we used equation(6) where $f= 30$ kHz, $\sigma_i = 10^{-5}$ S/m,
 390 and we obtained $S = 1.005$ for the night. Substituting the S value in equation (6), gives a
 391 phase velocity around 2.98×10^8 m/s for the night.

392 Substituting the above phase velocity values in equation (14) gives distance estima-
 393 tions described below in equation (20).

$$394 \quad d(\text{night}) = 6.66 \times 10^9 (t_{ELF} - t_{VLF}) \quad (20)$$

396 Note that equation (20) only applies for sferics in which height of the ionosphere is con-
 397 stant in their propagation path, i.e., those sferics that do not cross the day–night termi-
 398 nator. Figures 12 shows a histogram of the estimated error for lightning distance for a
 set of 100 sferics occurred in night. As seen from Figures 12, distance estimation has an



395 **Figure 12.** A histogram of the error values for distance approximation for 100 sferics

399 average error of $\sim 6.7\%$ with $\sim 5\%$ standard deviation. We further compared our time
 400 emission estimations with those of the NLDN for the same strikes. It is worth noting that
 401 this average error is in percentage of the actual distance between station and the lightning
 402 stroke and would increase as station-lightning stroke distance increases.
 403

407 The histogram of the time emission approximation error is shown in Figure 13. The
 408 result shows $\sim 2 \times 10^{-4} \%$ average error and $\sim 3 \times 10^{-4} \%$ standard deviation. The coverage

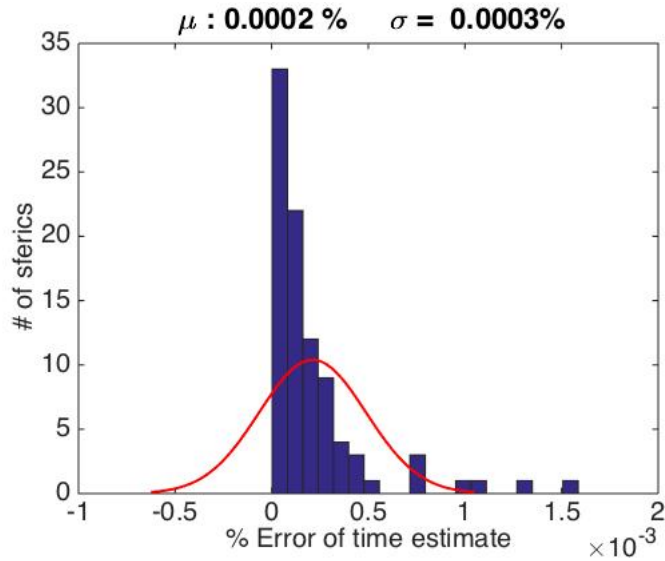


Figure 13. A histogram of error values for time estimation for 100 sferics

404

409 range of the method can be estimated using distribution of the lightning's peak currents
 410 and also minimum detectable peak current around the globe. Sondrestrom station mostly
 411 covers lightnings occurring in the Northern American and Western European regions (
 412 Mackay C.E.J, et al., 2012). The error estimation results for the direction finding method
 413 described in section (6-4), are also shown in Figure 14a. This method yields average error
 414 $\sim 6.7\%$ with $\sim 17.6\%$ standard deviation. Using proposed improvements in section 6-4,
 415 we also computed a histogram of the error for direction approximation for same set of
 416 sferics. As seen in Figure 14b the average error dropped by $\sim 5.4\%$ in comparison with
 417 the method proposed by *Said, R. K. et al.*, 2010.

418

8 Conclusion

419

420

421

422

423

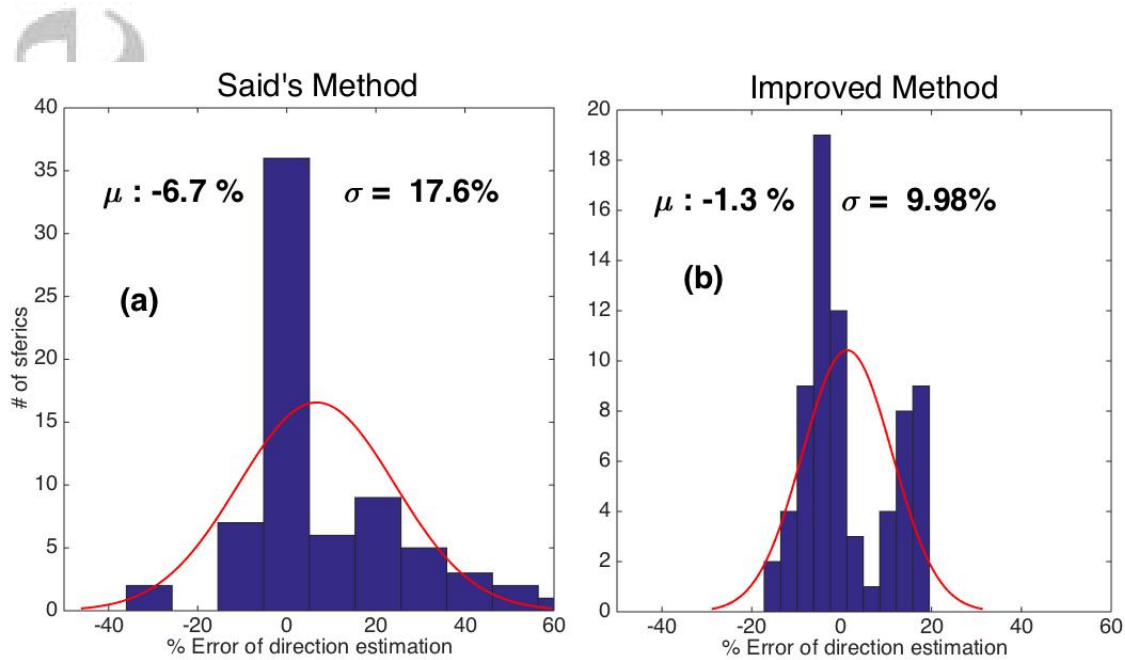
We have introduced a novel method to estimate the propagation distance and the emission time of sferics using recorded data from single station. Our method is more accurate and more widely applicable than the Ogawa method while being less resource intensive than other single-station methods (*Mackay C.E.J, et al.*, 2012) as well as multi-station methods, like the NLDN.

424

425

426

These improvements were achieved first by making key observations into the time relationship between ELF and VLF components of sferics. With these observations and the Galejs method for approximating the phase velocities we estimated the propagation



405 **Figure 14.** A histogram of error values for direction estimations for 100 sferics using *Said, R. et al., 2010*
 406 (a), using modified MDF for single station (b)

427 distance of the sferics. Additional improvements were achieved by estimating the azimuth
 428 of the sferic by considering the whole sferic waveform and not just the VLF part.

429 In short, while our method may be less accurate than multiple station methods, it is
 430 more accurate and less resource intensive than previous single-station methods. Given the
 431 advantages of using single station measurements relative to using multiple-station methods
 432 such as reduced cost for building, maintenance, and synchronization of the stations, it is a
 433 great alternative to multiple- station methods in many applications where the precise loca-
 434 tion of individual lightning discharges is not the significant factor. Identifying lightning
 435 storm regions is the important factor where can be achieved using the proposed method by
 436 clustering the measurements of each single lightning within the storm.

437 Acknowledgments

438 Partial support for this research was provided by the Office of Polar Programs of the
 439 National Science Foundation through the award 1246040. The experimental data used to
 440 prepare figures are saved in: <https://zenodo.org/record/3563054.XegLqveIZhF>

References

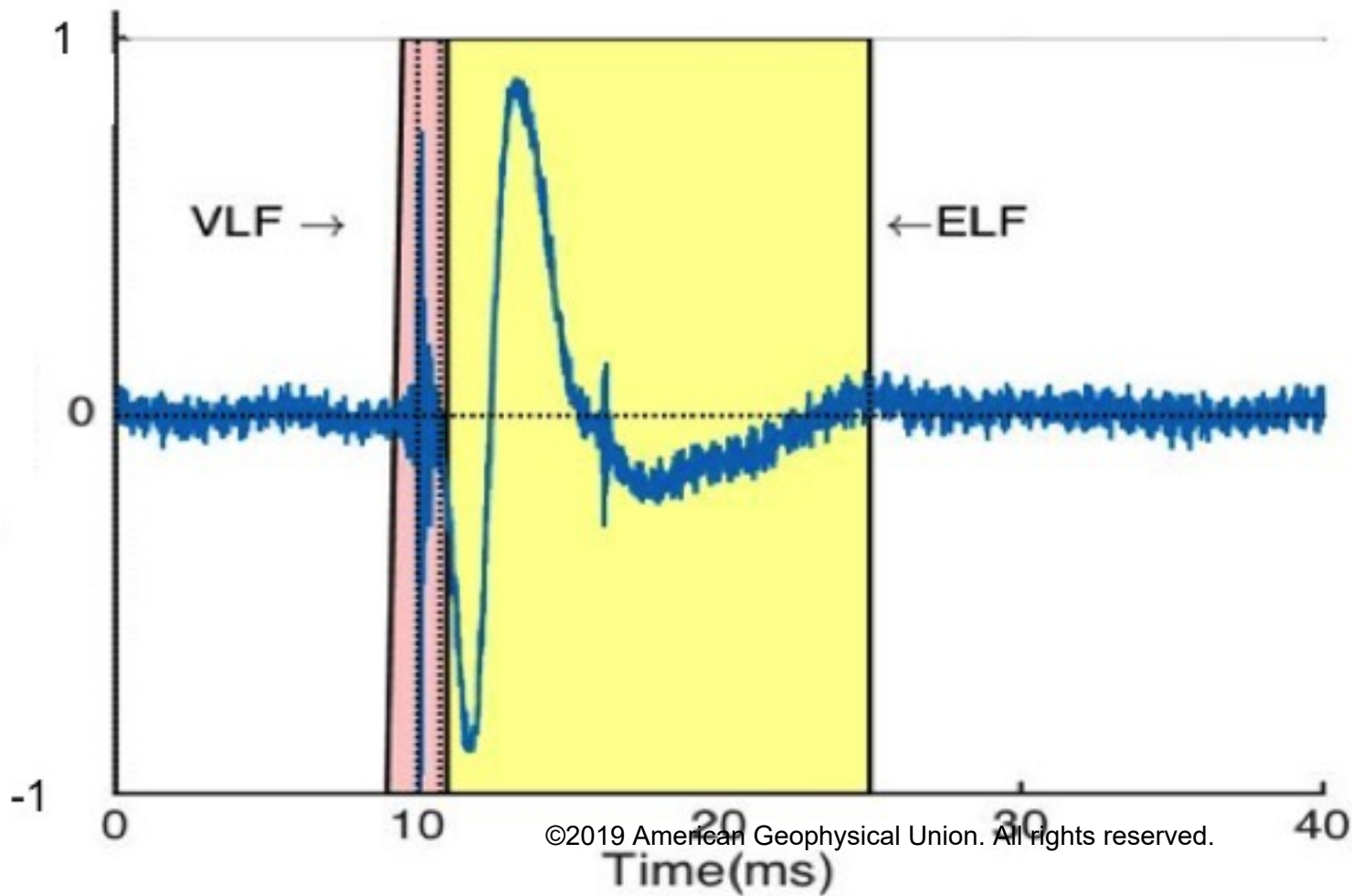
- 441
- 442 Burke, C. P., & Jones, D. L. (1995). Global radiolocation in the lower ELF frequency
443 band. *Journal of Geophysical Research: Atmospheres*, 100(D12), 26263-26271.
- 444 Cummins, K. L., & Murphy, M. J. (2009). An overview of lightning locating systems:
445 History, techniques, and data uses, with an in-depth look at the US NLDN. *IEEE Trans-*
446 *actions on Electromagnetic Compatibility*, 51(3), 499-518.
- 447 Füllekrug, M. (2017). Introduction to lightning detection. *Weather*, 72(2), 32-35.
- 448 Galejs, J. (1972). Terrestrial propagation of long electromagnetic waves: International
449 series of monographs in electromagnetic waves, Pergamon, 1972, Pages 74-149
- 450 Hughes, H. G., and R. J. Gallenberger (1974), Propagation of extremely low-
451 frequency(ELF) atmospherics over a mixed day-night path, *J. Atmos. Terr. Phys.*, 36
452 (10), 16431661, doi:DOI:10.1016/0021-9169(74)90202-5.
- 453 Inan, U. S., & Inan, A. S. (2000). *Electromagnetic waves*
- 454 Mackay, C., & Fraser-Smith, A. C. (2010). Lightning location using the slow tails of sfer-
455 ics. *Radio Science*, 45(5).
- 456 Mackay, C. E. J. (2012). *Locating Lightning from Slow-tail Measurements Recorded at a*
457 *Single Station* (Doctoral dissertation, Stanford University).
- 458 Murphy, M. (2018). *Locating lightning*. *Physics Today*, 71(3), 32-38.
- 459 Nag, A., Mallick, S., Rakov, V. A., Howard, J. S., Biagi, C. J., Hill, J. D., ... & DeCarlo,
460 B. A. (2011). Evaluation of US National Lightning Detection Network performance
461 characteristics using rocket-triggered lightning data acquired in 2004-2009. *Journal of*
462 *Geophysical Research: Atmospheres*, 116(D2).
- 463 Nag, A., Murphy, M. J., Schulz, W., Cummins, K. L. (2015). Lightning locating systems:
464 Insights on characteristics and validation techniques. *Earth and Space Science*, 2(4), 65-
465 93.
- 466 Ogawa, T., & Komatsu, M. (2007). Analysis of Q burst waveforms. *Radio Science*, 42(2).
- 467 Price, C., Asfur, M., Lyons, W., & Nelson, T. (2002). An improved ELF/VLF method for
468 globally geolocating sprite-producing lightning. *Geophysical Research Letters*, 29(3).
- 469 Ramachandran, V., Prakash, J.N., Deo, A. and Kumar, S., 2007, July. Lightning stroke
470 distance estimation from single station observation and validation with WWLLN data.
471 In *Annales Geophysicae* (Vol. 25, No. 7, pp. 1509-1517).

- 472 Said, R. K., Inan, U. S., & Cummins, K. L. (2010). Long-range lightning geolocation us-
473 ing a VLF radio atmospheric waveform bank. *Journal of Geophysical Research: Atmo-*
474 *spheres*, 115(D23).
- 475 Said, R. K., Cohen, M. B., & Inan, U. S. (2013). Highly intense lightning over the oceans:
476 Estimated peak currents from global GLD360 observations. *Journal of Geophysical Re-*
477 *search: Atmospheres*, 118(13), 6905-6915.
- 478 Said, R.K., (2017). Towards a global lightning locating system. *Weather*, 72(2), 36-40.
- 479 Wait, J. R. (1960). Terrestrial propagation of very-low-frequency radio waves, a theoretical
480 investigation. *J. Res. Nat. Bureau Stand*, 64, 153
- 481 Wait, J. R. (1960). On the theory of the slow-tail portion of atmospheric waveforms. *Jour-*
482 *nal of Geophysical Research*, 65(7), 1939-1946.
- 483 Wait, J. R. (1970). *Electromagnetic Waves in Stratified Media*, Pergamon.

Figure.

Accepted Article

Magnetic field

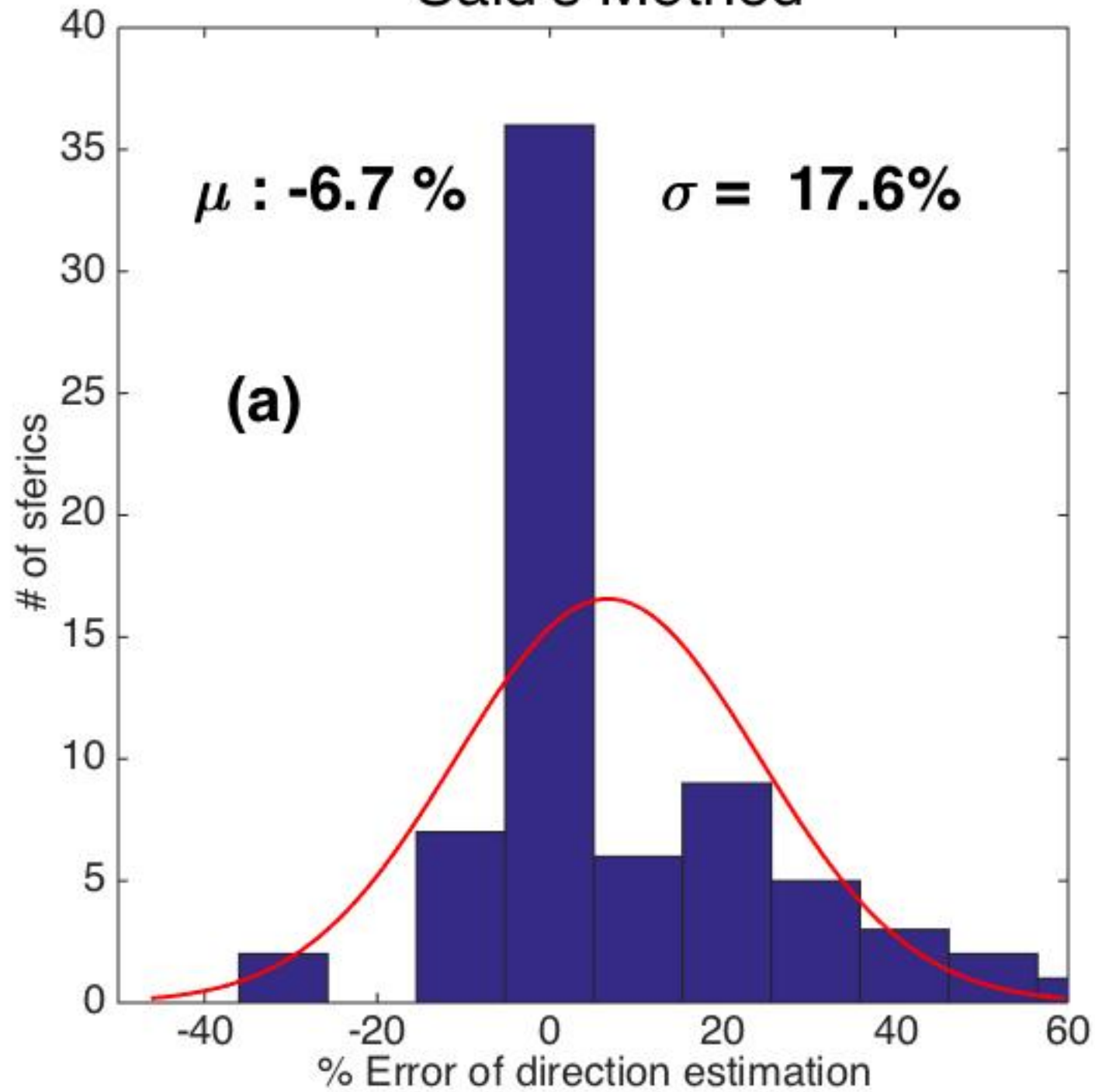


©2019 American Geophysical Union. All rights reserved.

Figure.

Accepted Article

Said's Method



Improved Method

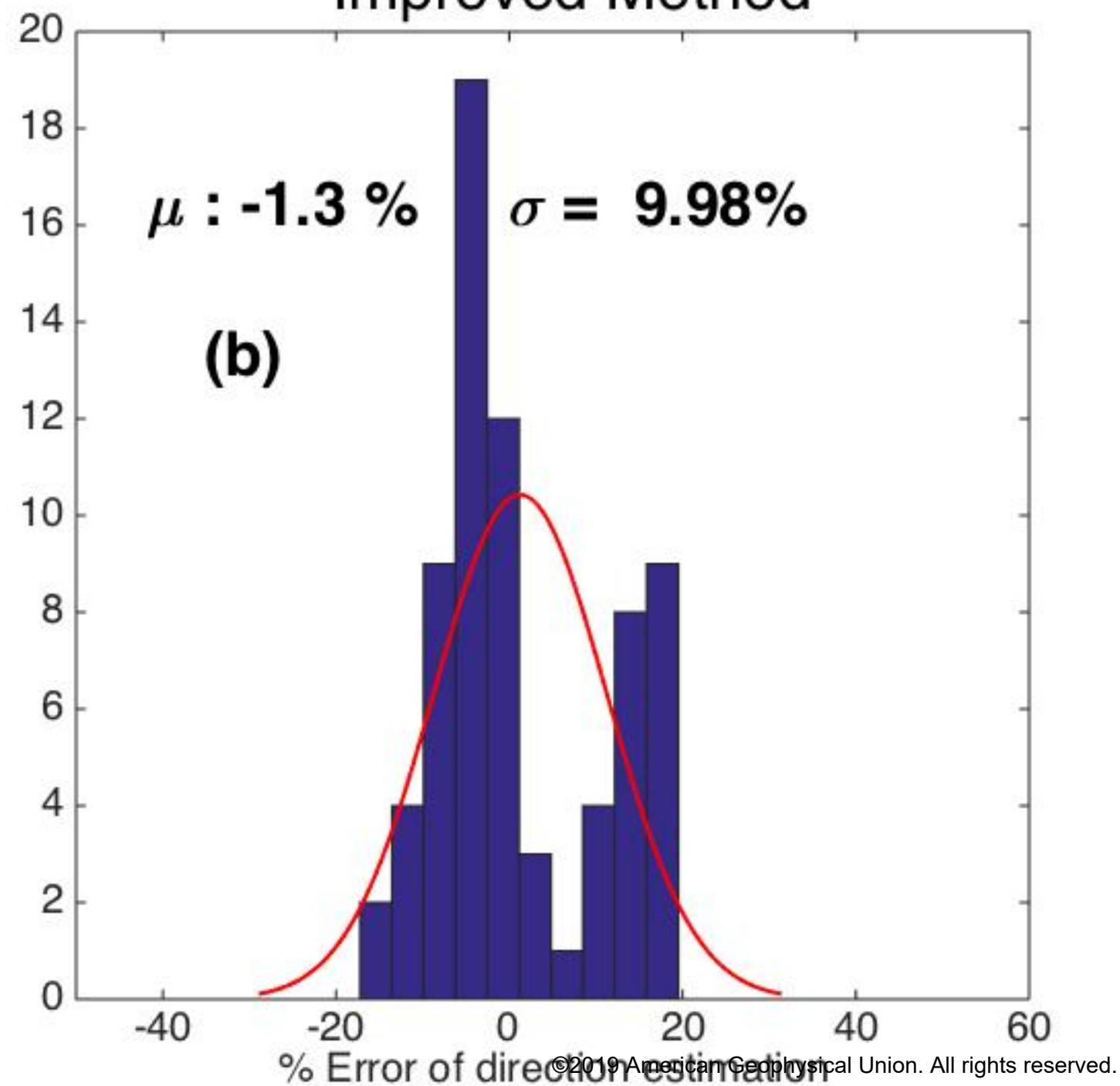
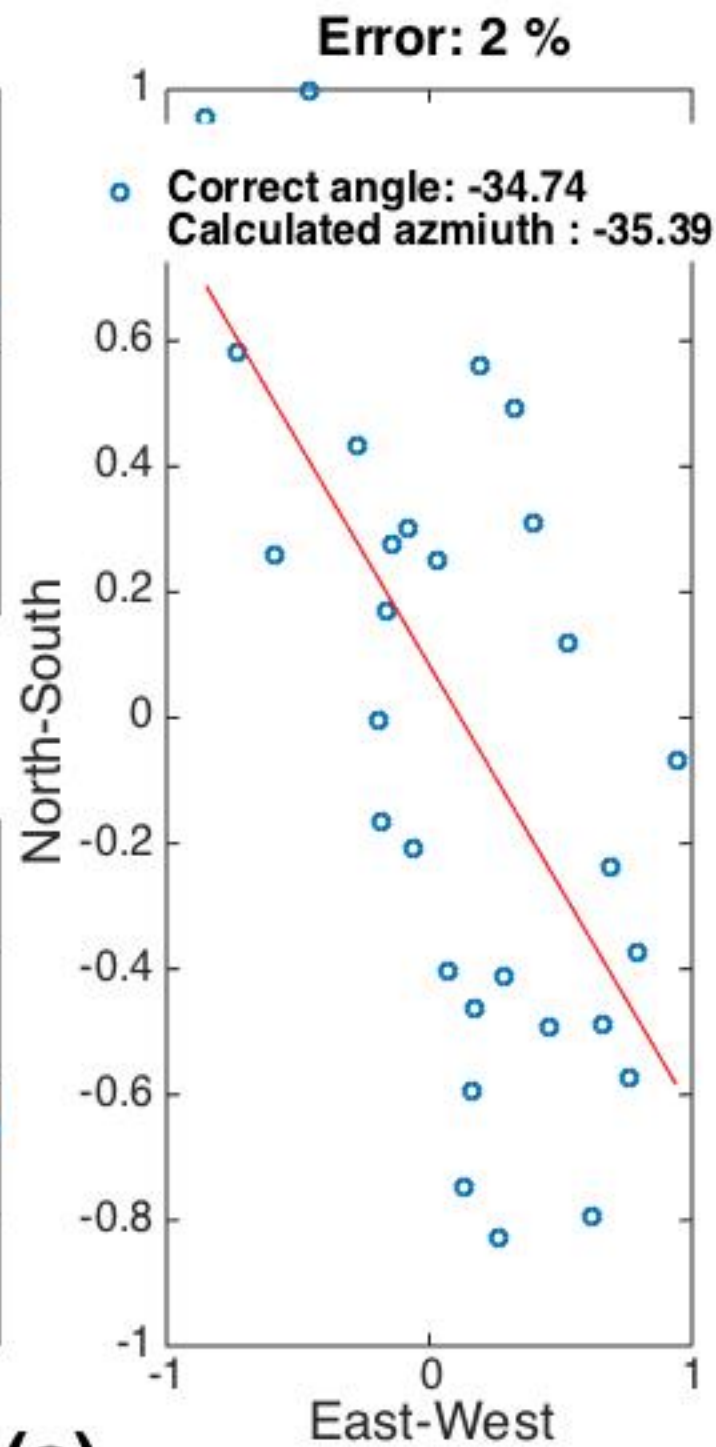
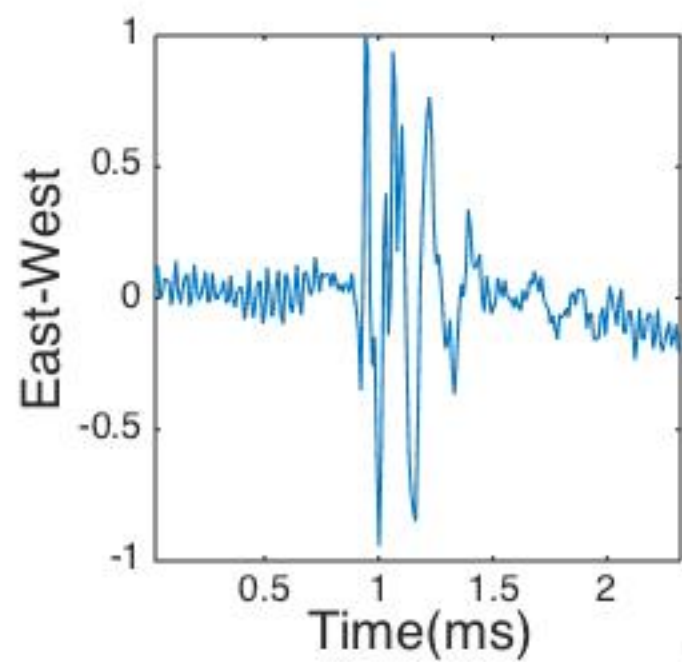
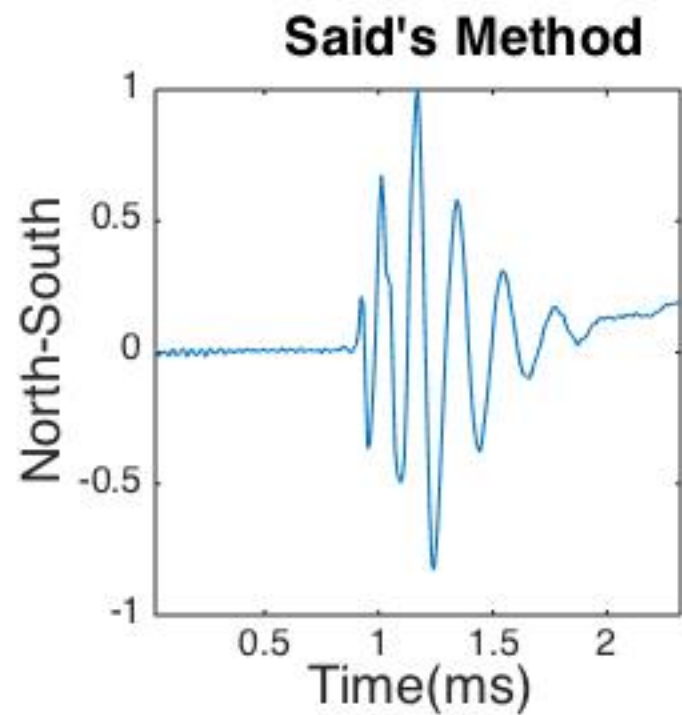
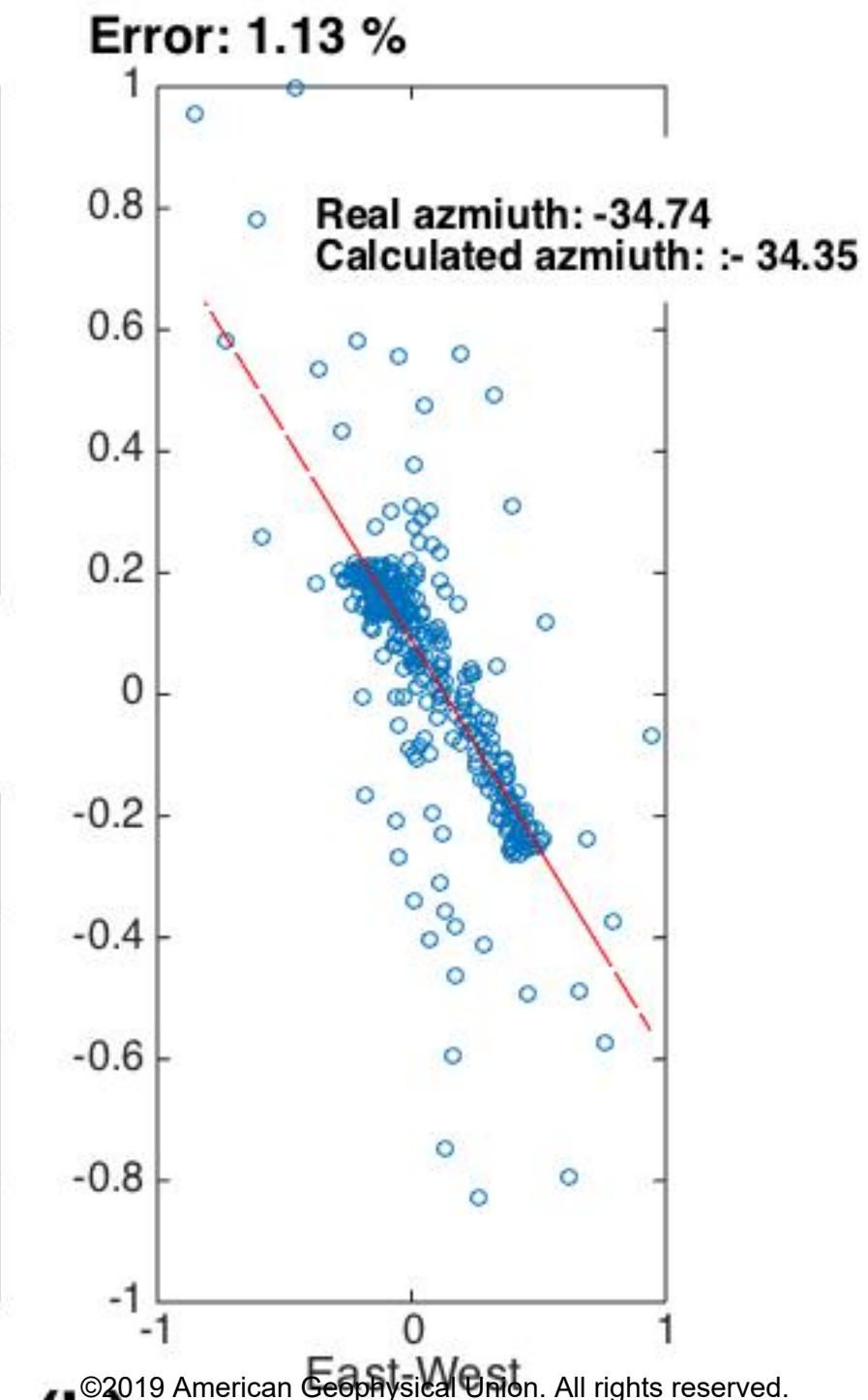
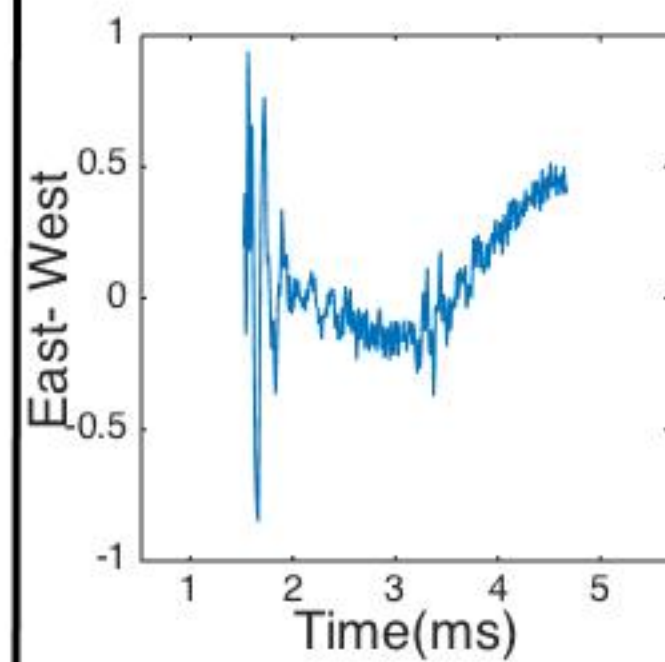
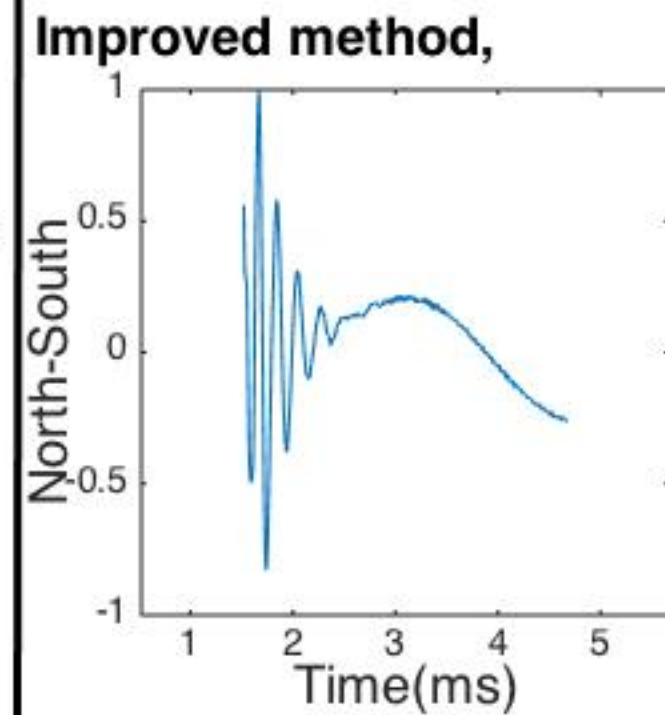


Figure.

Accepted Article



(a)



(b)

Figure.

Accepted Article

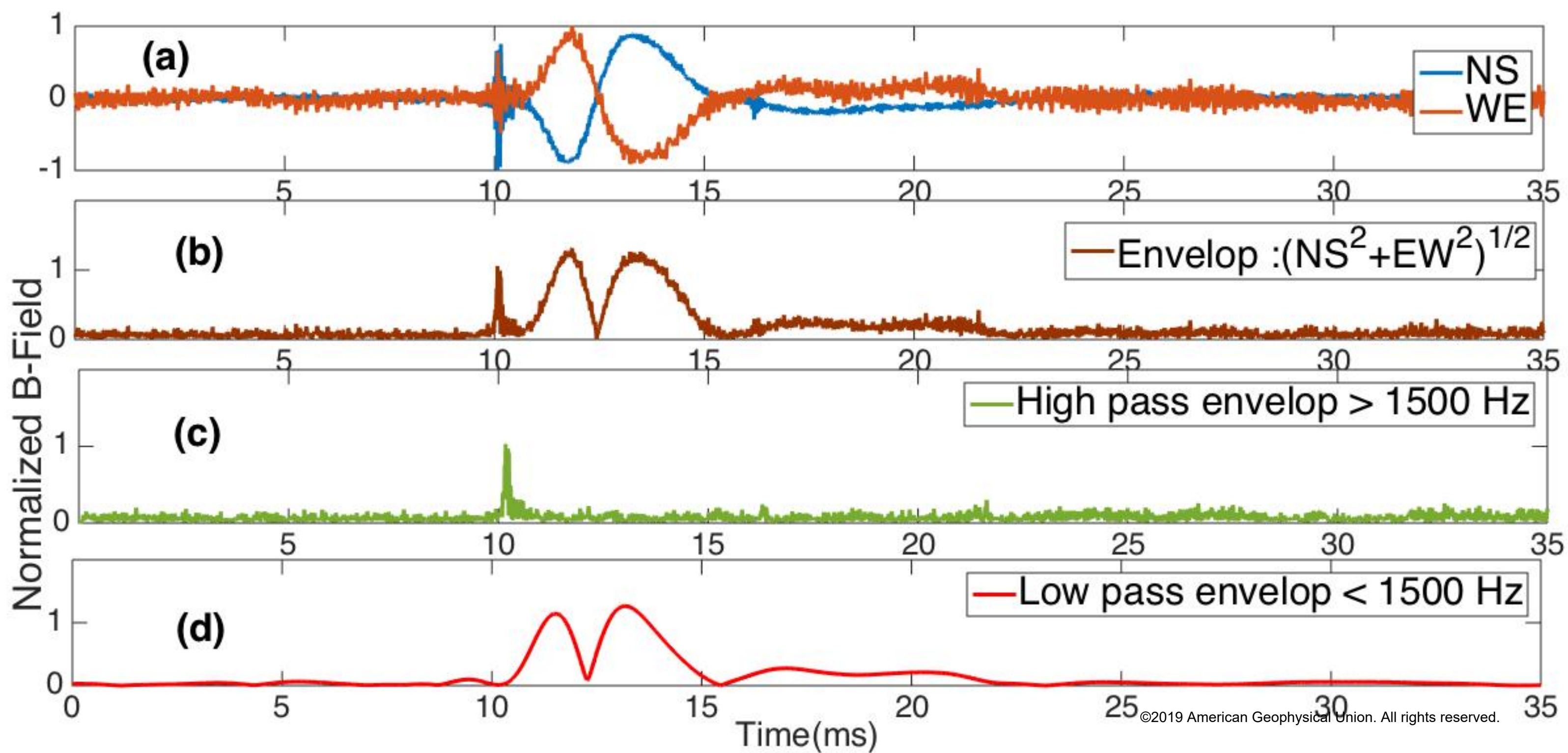


Figure.

Accepted Article

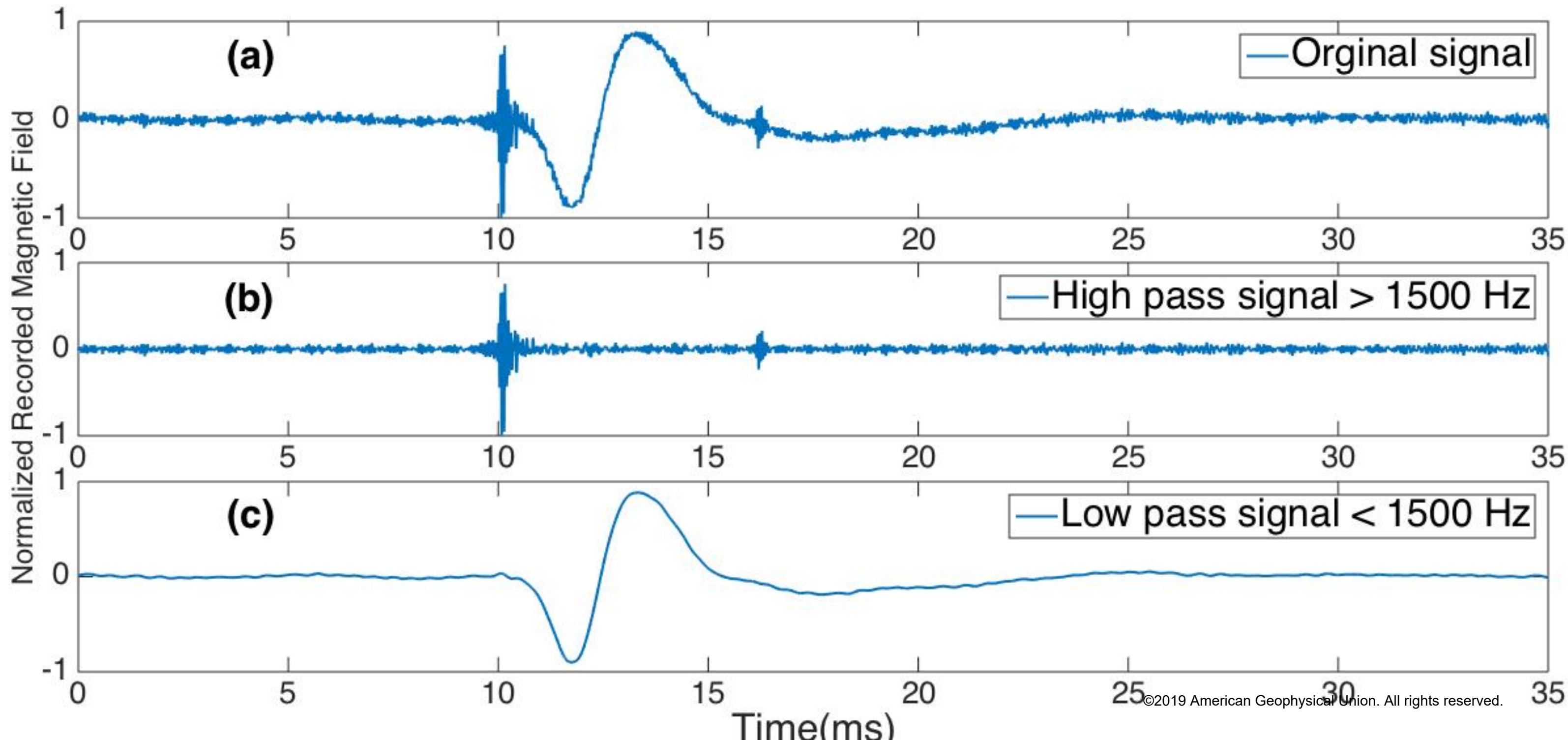


Figure.

Accepted Article

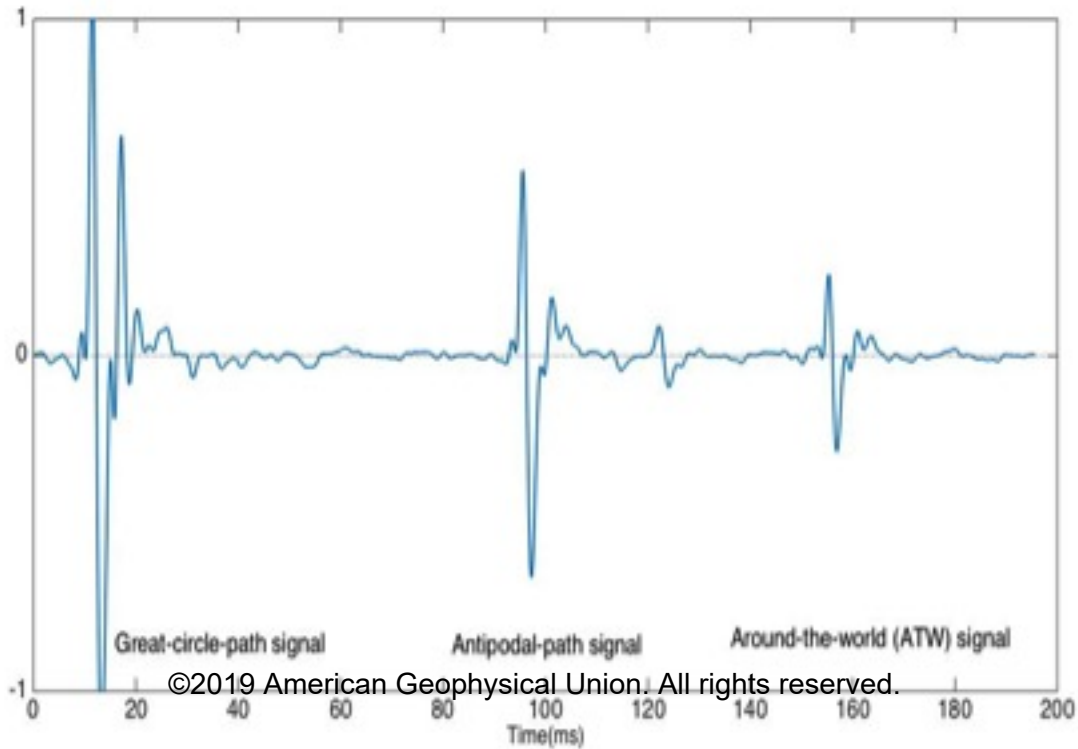


Figure.

Accepted Article

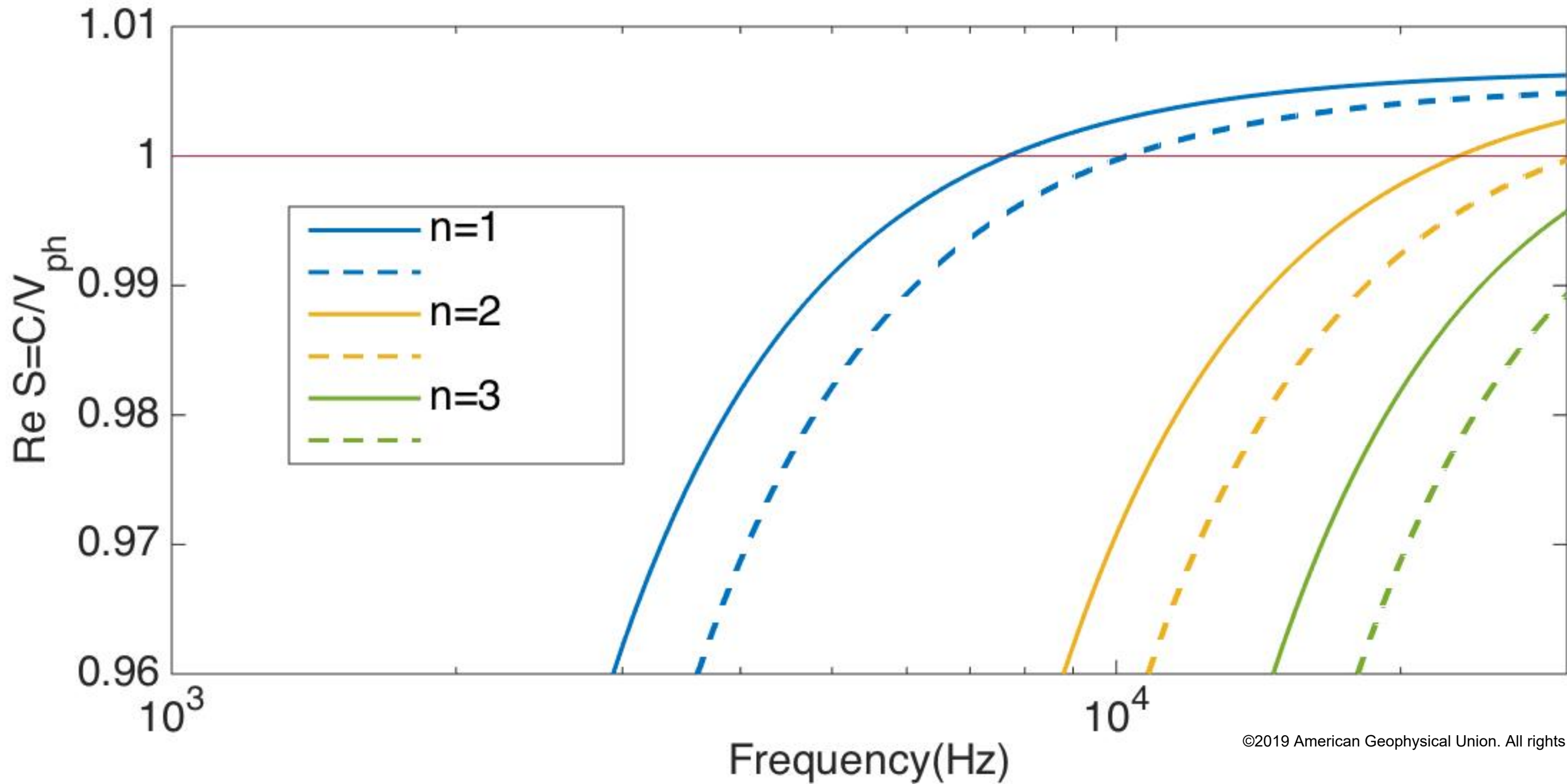


Figure.

Accepted Article

Ionosphere

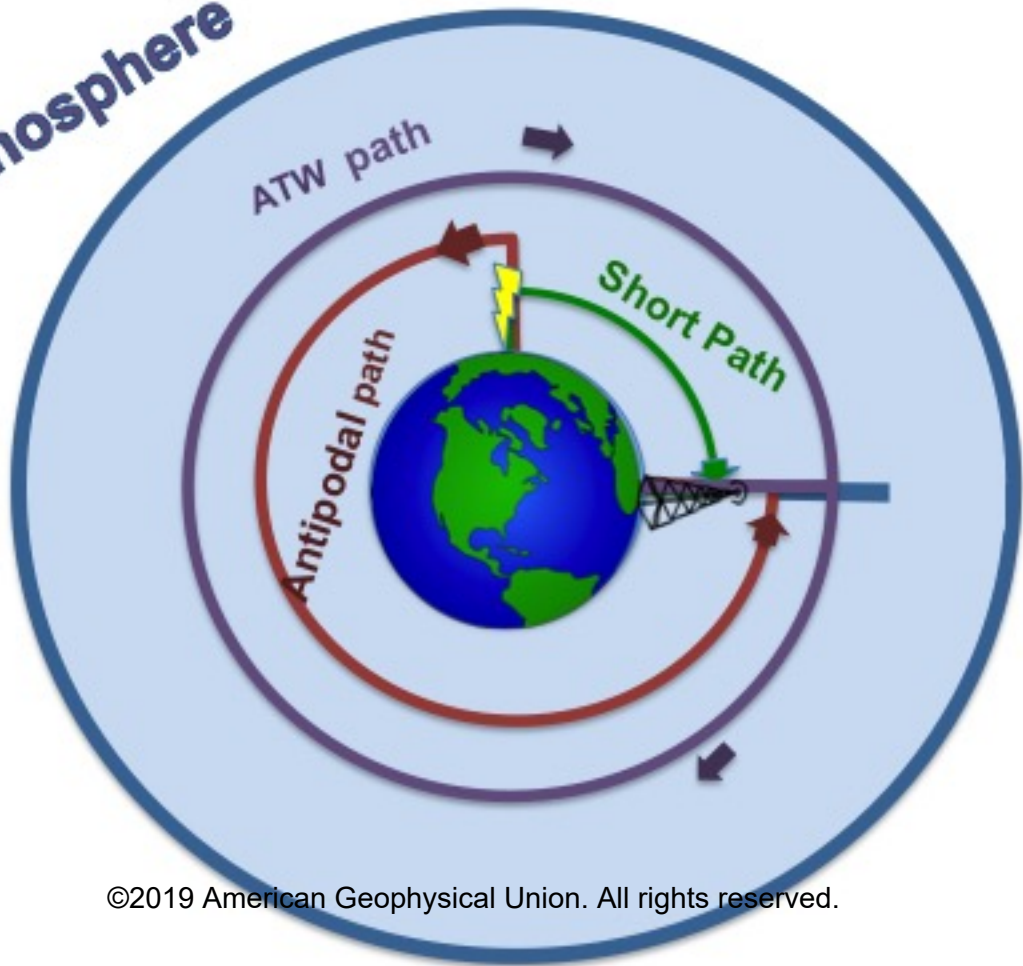
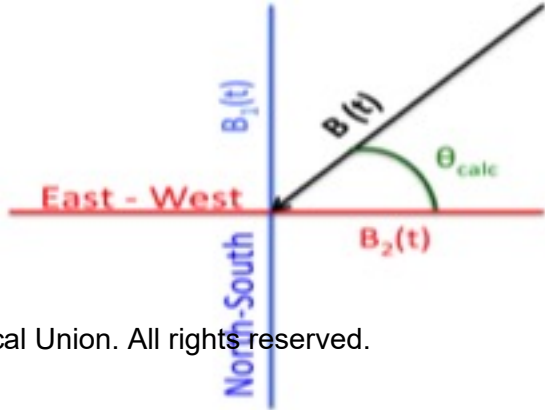


Figure.

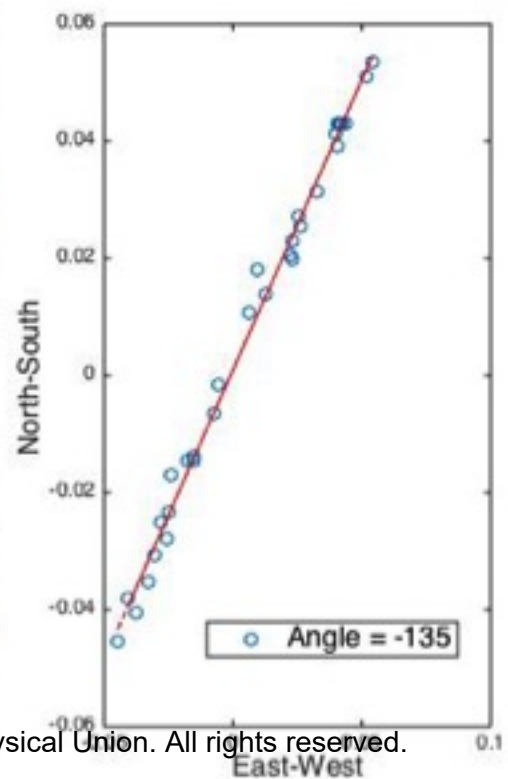
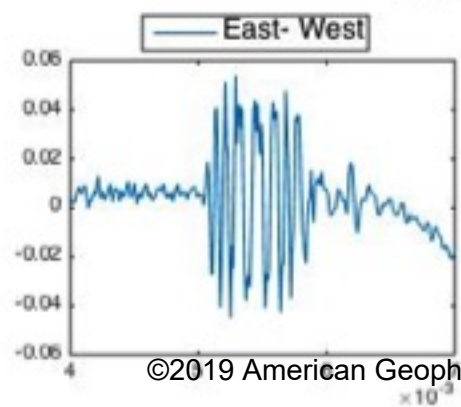
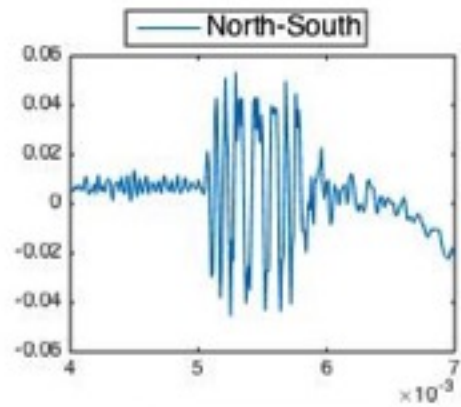
Accepted Article



cal Union. All rights reserved.

Figure.

Accepted Article



©2019 American Geophysical Union. All rights reserved.

Figure.

Accepted Article

$\mu : 6.7\%$ $\sigma = 5\%$

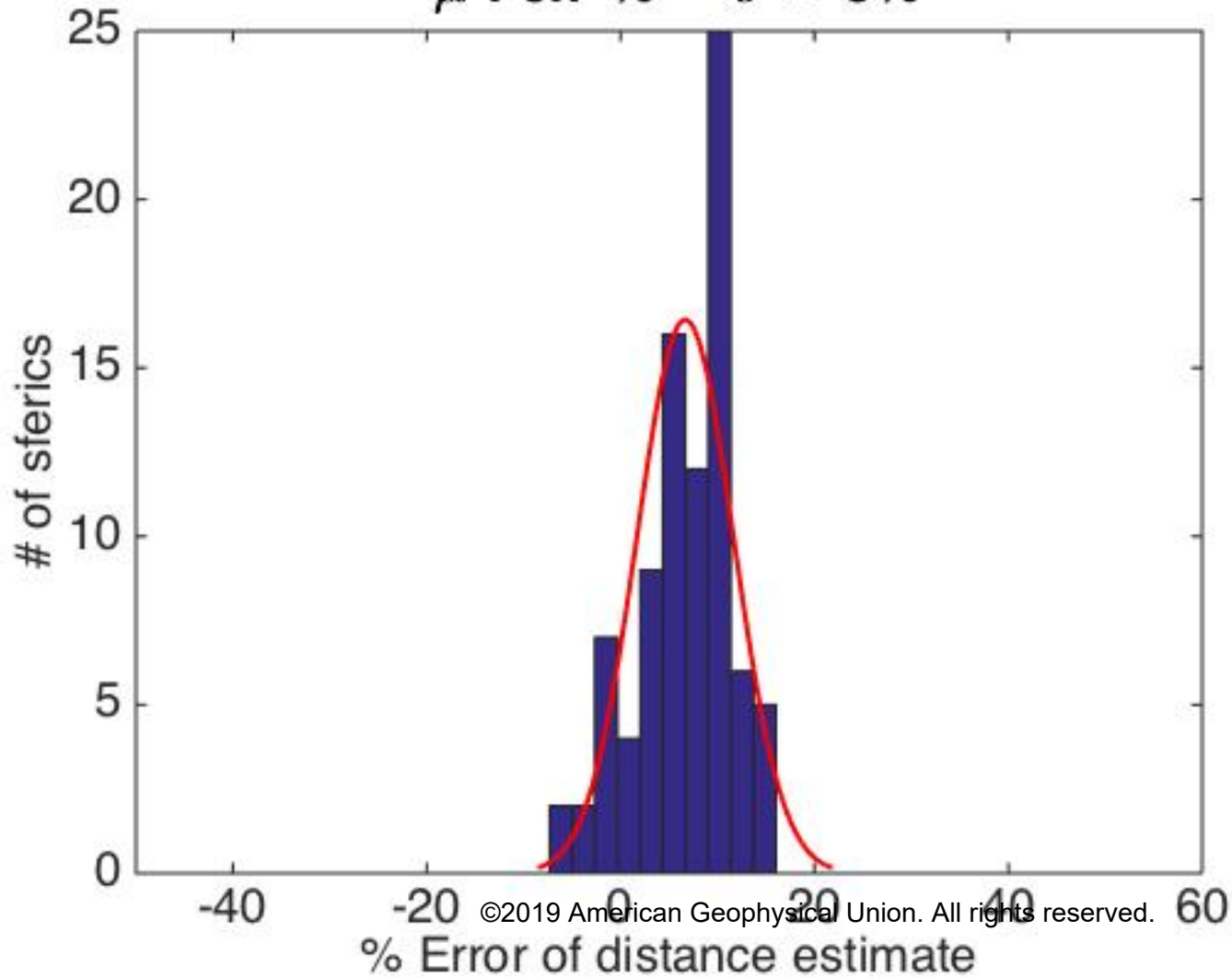


Figure.

Accepted Article

$\mu : 0.0002\%$ $\sigma = 0.0003\%$

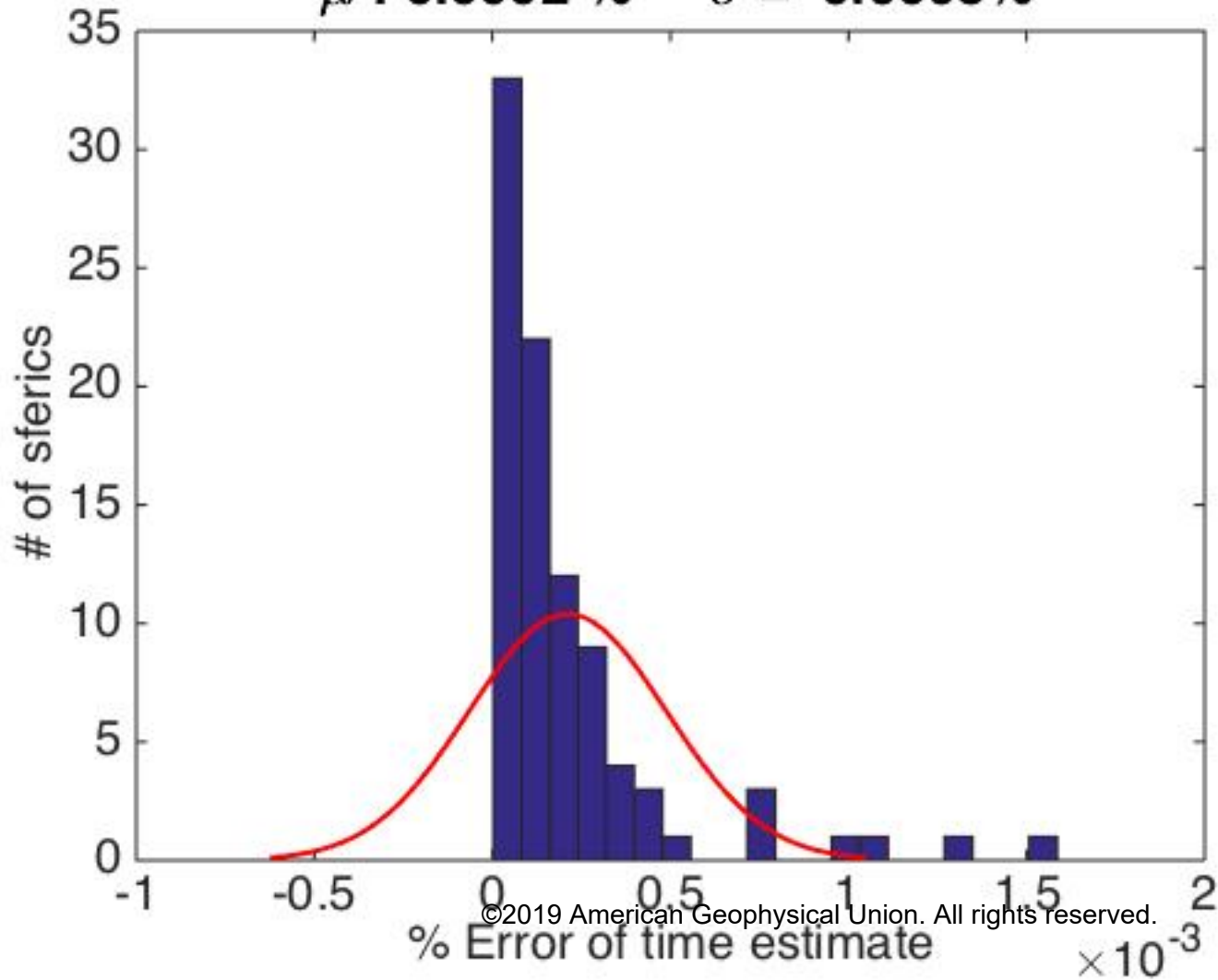
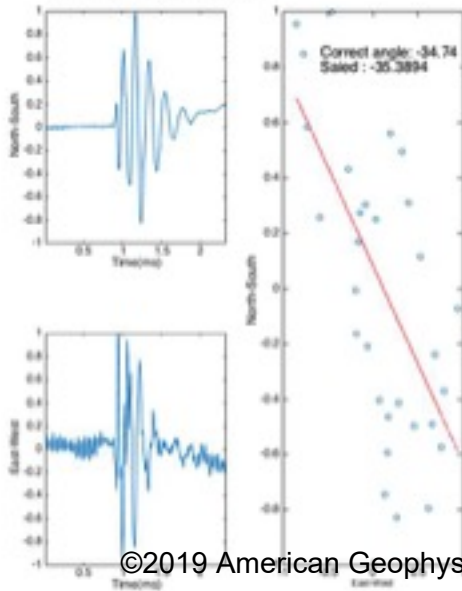


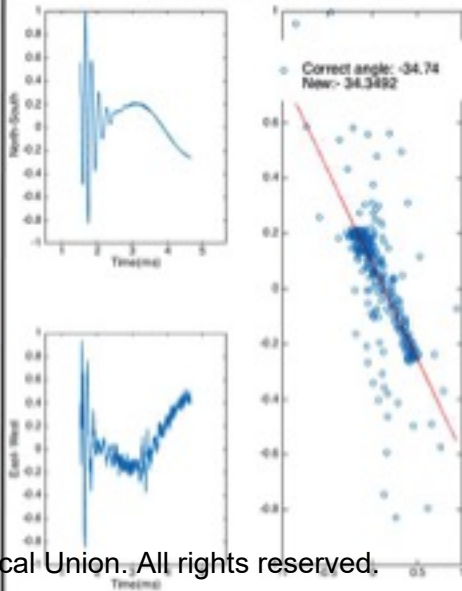
Figure.

Accepted Article

Error Saed Method: 2 %



Error Our method: 1.13 %



©2019 American Geophysical Union. All rights reserved.

Figure.

Accepted Article

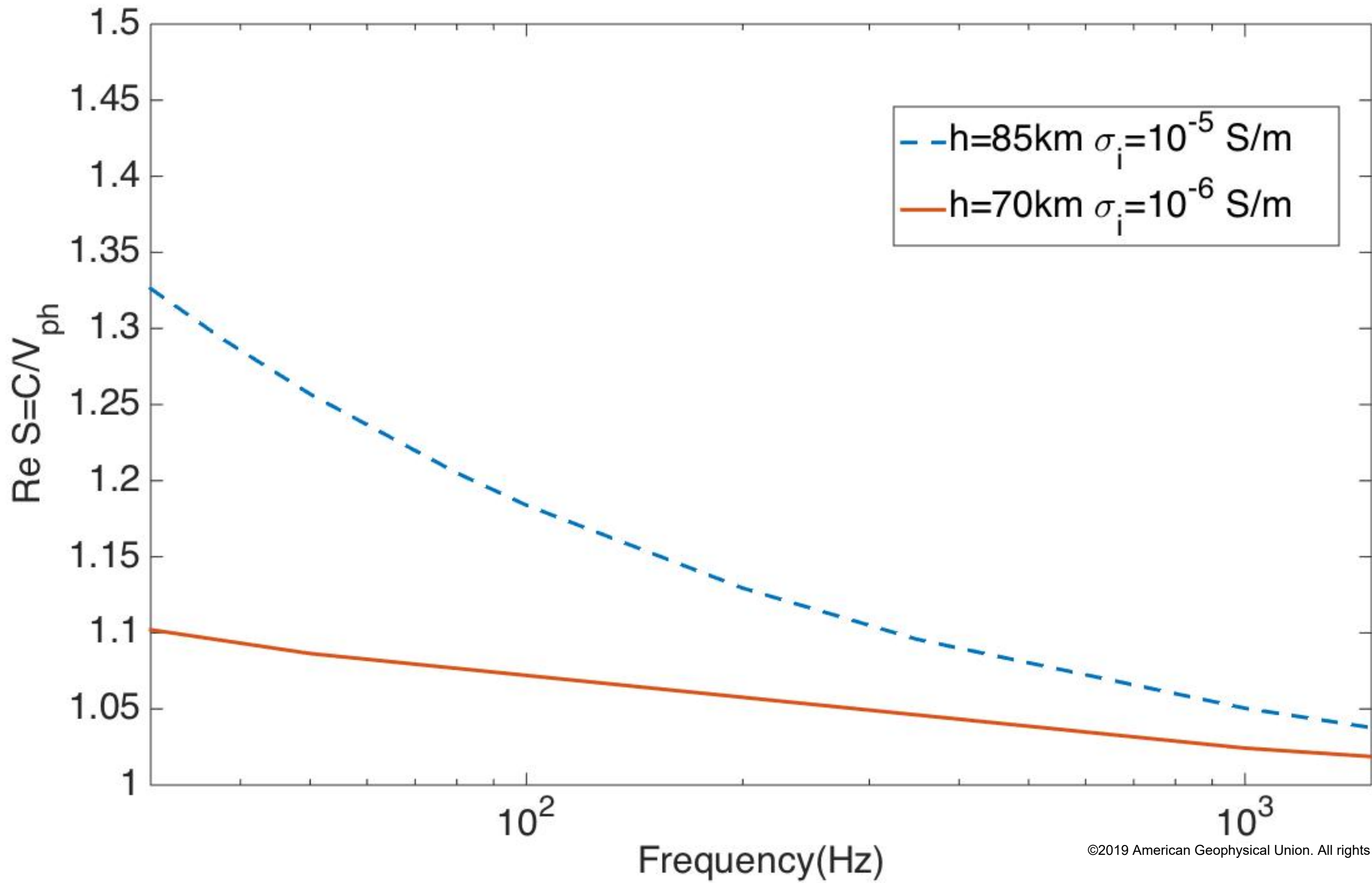


Figure.

Accepted Article

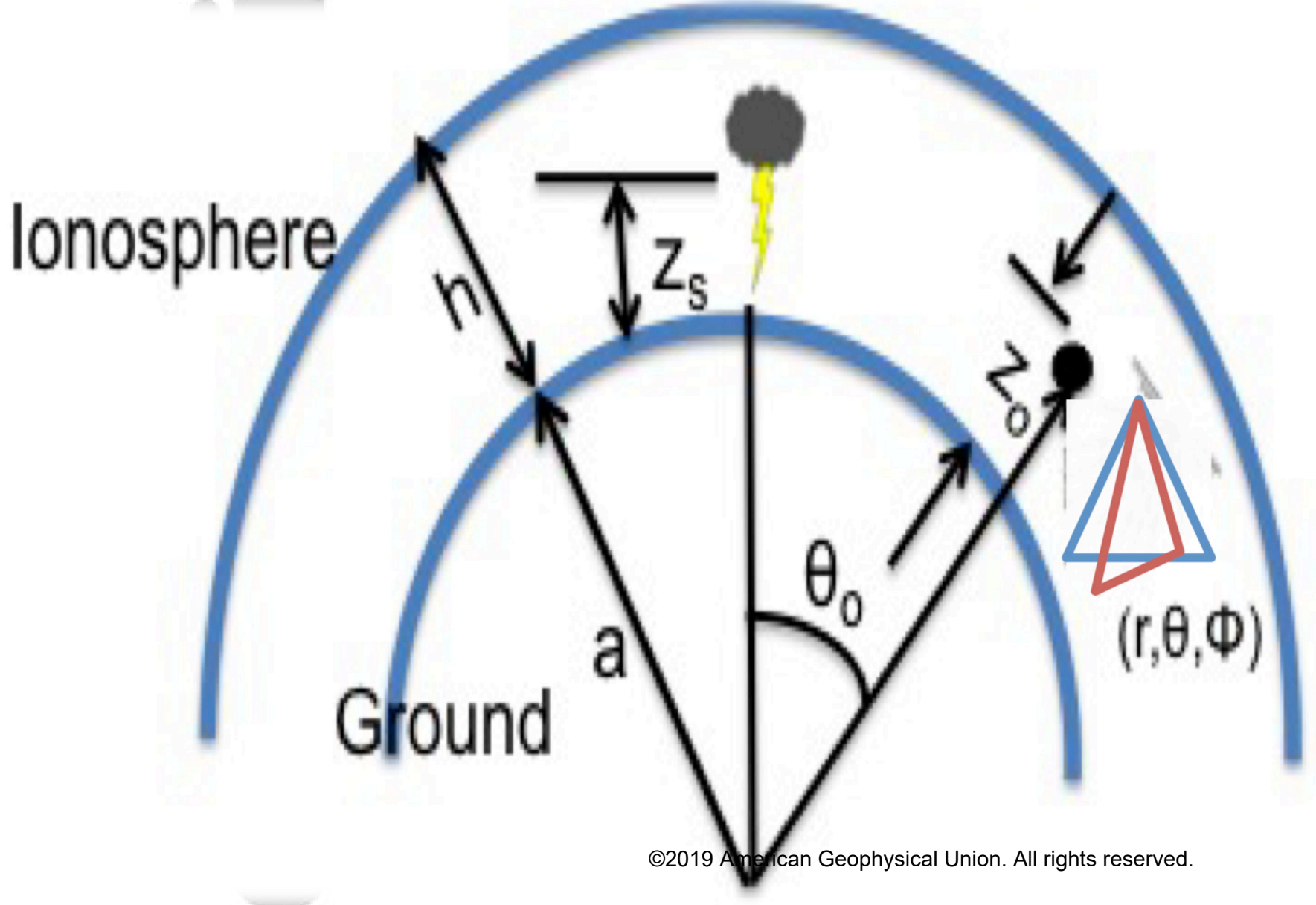


Figure.

Accepted Article

Magnetic field

